



POLITECNICO
MILANO 1863

Dipartimento di Elettronica, Informazione e Bioingegneria

Master Degree in Music and Acoustic Engineering

Modal analysis of classical guitar soundboard with parametric shape and fan bracing

by:
Mattia Vassena

matr.:
928050

Supervisor:
Fabio Antonacci

Co-supervisor:
Sebastián González

Academic Year
2020-2021



POLITECNICO
MILANO 1863

Dipartimento di Elettronica, Informazione e Bioingegneria

Master Degree in Music and Acoustic Engineering

**Analisi modale della tavola
armonica della chitarra
classica con forma
parametrica e catenatura a
ventaglio**

Candidato:
Mattia Vassena

matr.:
928050

Relatore:
Fabio Antonacci

Co-relatore:
Sebastián González

Anno accademico
2020-2021

Abstract

Guitar makers modify instruments to improve their sound quality, meet the needs and preferences of musicians, and make them suitable for contemporary playing environments. Claims about such improvements are often based on simple listening, without objective measurable results. The sound of the instrument is affected by the choices made in the design and building phases, so it is important to know the consequences on the vibrational behavior of the instrument brought by these factors.

In this work of thesis, we analyze the effect of the outline and the bracing features on the vibration modes of the guitar soundboard. To do so, we have built a virtual model of a Torres guitar soundboard and parameterized its shape, then we added the fan bracing parameterizing also the layout and the size of the struts in the lower bout. We generated several samples of soundboards through the variation of such parameters and performed Finite Element Modal Analysis on all of them to obtain their vibration modes and the natural frequencies.

Finally, we performed regression analysis on the results of the simulations. The regression coefficients constitute a model through which we can predict the natural frequencies of a soundboard knowing only its geometrical parameters. We use the regression coefficients also to measure the weight of the parameters on the variation of the frequencies, and verified that the main contributions corresponded with higher correlations. Our results indicate a generally lower contribution of the braces on the eigenfrequencies if compared to the variations of the shape, but highlighted the modes that are more affected by the changes in the bracing layout.

The regression model we found can help guitar makers predict the vibrational behavior of a soundboard with fan bracing before building it and give a tangible measure of the impact of different construction choices. With this type of study, we are moving towards better tonal characterizations of guitars and many other musical instruments.

Sommario

I liutai modificano gli strumenti per migliorarne le qualità sonore, per incontrare necessità e preferenze dei musicisti e per adattarne le caratteristiche per gli ambienti di esecuzione contemporanei. Le affermazioni su tali migliorie sono spesso basate sul semplice ascolto, prive di risultati misurabili ed oggettivi.

Il suono di uno strumento è influenzato dalle scelte fatte in fase di progetto e costruzione, è dunque importante conoscere le conseguenze sul comportamento vibrazionale dovute a questi fattori.

In questa tesi analizziamo gli effetti delle caratteristiche del contorno e della catenatura della tavola armonica sui suoi modi di vibrazione. Per questa analisi abbiamo costruito un modello virtuale di una tavola di chitarra Torres e abbiamo parametrizzato la sua forma; successivamente abbiamo aggiunto la catenatura e parametrizzato la disposizione e le dimensioni dei rinforzi nella parte inferiore del corpo. Attraverso la variazione di tali parametri, abbiamo generato molteplici campioni di tavole. Abbiamo eseguito un'analisi modale su modelli a elementi finiti di tutti i campioni generati, ottenendo i loro modi di vibrazione e le relative frequenze naturali, e controllando la presenza di inversioni nell'ordinamento per frequenza dei modi di vibrazione rispetto al modello di riferimento. Infine abbiamo eseguito un'analisi di regressione sui risultati delle simulazioni. I coefficienti di regressione costituiscono un modello attraverso il quale possiamo predire le frequenze naturali di una tavola armonica conoscendo solo i parametri geometrici che la descrivono. Abbiamo usato i coefficienti di regressione anche per misurare il peso dei diversi parametri sulla variazione delle autofrequenze, verificando che i contributi principali corrispondessero con correlazioni più alte.

I nostri risultati indicano che le catene contribuiscono meno alla modifica delle autofrequenze rispetto alle variazioni della forma della tavola, ma hanno un grado di influenza differente nei diversi modi di vibrazione.

Il modello di regressione proposto può essere d'aiuto per i liutai nella predizione del comportamento vibratorio di una tavola armonica con catenatura a ventaglio e dà una misura tangibile dell'impatto delle varie scelte costruttive. Con questo tipo di studio, stiamo procedendo verso una migliore caratterizzazione del suono della chitarra e di molti altri strumenti musicali.

Acknowledgements

First, I would like to thank my supervisor Professor Fabio Antonacci and my co-supervisor Sebastián González for giving me the opportunity to research this fascinating topic and for being reliable advisors throughout the whole work.

I would also like to thank all the people of the Musical Acoustics Lab for caring about my research and for sharing their expertise with me. Thanks, in particular, to my colleague Davide Salvi for sharing useful material and valuable suggestions from his research on violins.

Thanks to my colleague Tommaso Sciotto and to my friend Riccardo Gilardi for giving me further tips to better draw up this document. And thanks, finally, to all my friends and family for the constant support.

M. V.

Contents

| | |
|--|-------------|
| Abstract | i |
| Sommario | iii |
| Acknowledgements | v |
| List of Figures | xi |
| List of Tables | xiii |
| Nomenclature | xv |
| 1 Introduction | 1 |
| 1.1 Aim of the Thesis | 1 |
| 1.2 Application Fields | 3 |
| 1.3 Thesis Outline | 3 |
| 2 State of the Art and Background | 5 |
| 2.1 The Classical Guitar and its Components | 6 |
| 2.1.1 The Strings | 8 |
| 2.1.2 The Bridge | 8 |
| 2.1.3 The Soundboard | 9 |
| 2.1.4 The Bracing | 9 |
| 2.2 State of the Art on Modal Analysis of String Instruments | 10 |
| 2.3 Background on Finite Element Method | 13 |
| 2.3.1 Theoretical Background on FEM | 14 |
| 2.3.2 The Finite Element Modal Analysis | 15 |
| 2.4 Concluding Remarks | 17 |
| 3 Building a Parametric Mesh of a Braced Guitar Soundboard | 19 |
| 3.1 Definition of the Geometrical Parameters | 20 |
| 3.1.1 Outline Parameters | 20 |
| 3.1.2 Bracing parameters | 22 |
| 3.1.3 From the Torres Reference Model to a Dataset of Guitar Plates | 25 |
| 3.2 Creation of the Soundboard Mesh | 27 |
| 3.3 Creation of the Bracing Mesh | 30 |

| | | |
|----------|---|-----------|
| 3.3.1 | Braces in the Upper Bout | 30 |
| 3.3.2 | Braces in the Lower Bout | 33 |
| 3.4 | Concluding Remarks | 35 |
| 4 | Finite Element Modal Analysis of the Soundboard | 37 |
| 4.1 | Performing the Eigenfrequency Study in COMSOL | 38 |
| 4.1.1 | Mesh Parts | 38 |
| 4.1.2 | Geometry | 39 |
| 4.1.3 | Materials | 39 |
| 4.1.4 | Solid Mechanics | 40 |
| 4.1.5 | Eigenfrequency Study | 40 |
| 4.1.6 | Results | 40 |
| 4.1.7 | LiveLink™ scripting | 41 |
| 4.2 | Classification of the Vibration Modes | 41 |
| 4.3 | Eigenfrequencies Prediction from Geometrical Features | 45 |
| 4.4 | Bracing Influence on Eigenfrequencies | 50 |
| 4.5 | Concluding Remarks | 54 |
| 5 | Conclusions and Future Works | 55 |
| 5.1 | Future Works | 56 |
| | Appendices | 57 |
| A | Tables of the Regression Coefficients | 57 |

List of Figures

| | | |
|-----|---|----|
| 2.1 | Exploded view of a classical guitar [1]. | 7 |
| 2.2 | Different bracing systems for classical guitars. From left to right: Torres, lattice, Kasha and radial. | 10 |
| 2.3 | Chladni patterns of a soundboard mounted on a guitar body, excited at two different frequencies [2] | 12 |
| 2.4 | The function u (solid blue line) is approximated with u_h (dashed red line), which is a linear combination of partially overlapping piecewise linear basis functions ψ_i indicated in black (the shape of a single contribution ψ_1 as an example is represented by the cyan triangle). The coefficients are denoted by u_0 through u_7 . [3] | 15 |
| 3.1 | Definition of the outline. In the left image the thick blue lines represent the constraints on which the outline overlaps. The dashed lines in the right image represent the resulting outline and soundhole. | 21 |
| 3.2 | Outline parametrization. The variable parameters are indicated in green, the constant parameter is indicated in red. The y axis is highlighted with a black dashed line and constitutes an axis of symmetry for the soundboard. | 22 |
| 3.3 | Thickness of the reference soundboard with bracing | 23 |
| 3.4 | Orthogonal views of a brace shape: longitudinal view on the left and cross-section on the right. The surface of contact with the plate is shown flat but actually follows the light curvature of the soundboard. The parameters h_{\min} and h_{\max} define the thickness of the brace at different points and w defines its width. | 24 |
| 3.5 | The bracing orientations are driven by two independent angles, depicted in green. The angle α_K is a constant term to get the angle of the outermost fan α_{out} from the parameter α_{fan} | 25 |
| 3.6 | Four sample shapes from the dataset with $\sigma = 0.05$. The full set of parameters in table 3.1 is varying, the number of braces is kept constant. | 27 |
| 3.7 | Soundboard points: z axis magnified. The (x, y) plane is centered in the center of the curve. | 28 |

| | | |
|------|--|----|
| 3.8 | Points of the cross-sections of a brace in two different parts of the longitudinal shape. The blue points are in contact with the soundboard and the red points create the opposite face. The cross-section in the left picture is the central one ($x_n = x = 0$): it reaches the maximum thickness of the brace h_s . The cross-section in the right picture is near the edge ($x_n \approx 1$), where the curved part flattens. | 31 |
| 3.9 | Curvature of braces along the longitudinal direction (normalized). In the interval $[0, x_s]$ the brace thickness is controlled by the gaussian curve. In the interval $[x_s, 1]$ also the scalloping is applied. | 32 |
| 3.10 | Position of the braces next to the soundhole. The dashed lines are centerlines of the brace and the soundhole. The distance d from the soundhole to the waist depends on the parameters of the outline. | 32 |
| 3.11 | Scheme of the bracing layout assembly. The distances d_i indicate that the centers of the fan braces, circled in black, are always placed in the middle of a line that goes from the lower braces to the upper y limit. The red values are the constants we used to locate p_{out} based on the lower braces position. | 34 |
| 4.1 | COMSOL Multiphysics workflow. The software is organized into nodes that are evaluated sequentially. Each of the 4 main nodes contains many sub-nodes, we have shown in the figure those on which we operate. | 38 |
| 4.2 | Histogram of the eigenfrequencies. Dataset of 1000 samples with all parameters variable ($\sigma = 0.05$). The different coloured distributions refer to the seven different vibration modes. | 42 |
| 4.3 | From left to right, modes 3 and 4 variants, belonging to the same sample | 43 |
| 4.4 | Fourier transform of the displacement data of modes 3 (0,2) and 7 (1,1). k_x and k_y represent the wave number of the spatial frequency bin in the two directions x and y | 44 |
| 4.5 | Performance of the quadratic regression incrementing the number of parameters from 1 to 7. Each increment involves the parameter that maximizes the R^2 index. The red line represents the maximum R^2 corresponding to the regression of all the 20 parameters listed in table 3.1 | 47 |
| 4.6 | Correlation coefficients of the 20 geometrical parameters listed in table 3.1 with the 7 eigenfrequencies. All parameters are varying with $\sigma = 0.05$ and described in table 3.1. | 48 |
| 4.7 | Histogram of the eigenfrequencies. Dataset of 1000 samples with only bracing parameters variable ($\sigma=0.2$). | 51 |

| | | |
|-----|--|----|
| 4.8 | Performance of the quadratic regression, incrementing the number of parameters from 1 to 7. Each increment involves the parameter that maximizes the R^2 index. The red line represents the maximum R^2 achieved with all the 8 parameters. | 52 |
| 4.9 | Correlation coefficients in the varying bracing case. The last three variables on the x axis are the total bracing volume V , the number of braces n and the ratio between the two. These parameters are derived from the other 8 ones, which are described in table 3.1 in the rows related to the bracing. | 54 |

List of Tables

| | | |
|-----|---|----|
| 3.1 | Summary of the geometrical parameters. Graphical representation of the parameters are shown in figure 3.2 for the outline and in figures 3.4 and 3.5 for the bracing. . . | 26 |
| 4.1 | Orthotropic material model for the soundboard | 39 |
| 4.2 | Isotropic material model for the braces | 40 |
| 4.3 | Modal shapes of the reference model. This model is not taken from the dataset, it is equivalent to a sample in which all the parameters are set to the mean value of their distributions. | 43 |
| 4.4 | Regression performance: R^2 values of quadratic regression for the 7 modes. All parameters varying ($\sigma=0.05$). | 46 |
| 4.5 | Standard deviation of the frequencies calculated with the numerical simulations, compared between the two datasets. Pedices indicate the number of varying parameters: σ_{20} refers to the completely variable dataset and σ_8 refers to the bracing varying one. The mean of the seven values of the standard deviation is expressed as μ_f | 50 |
| 4.6 | Regression performances: R^2 values of quadratic regression for the 7 modes. Eight parameters varying ($\sigma=0.2$) . | 51 |
| 1 | Linear terms \mathcal{B}_1 of regression coefficients, dataset of 20 varying parameters ($\sigma = 0.05$) | 57 |
| 2 | Quadratic terms \mathcal{B}_2 of regression coefficients, dataset of 20 varying parameters ($\sigma = 0.05$) | 58 |
| 3 | Linear terms \mathcal{B}_1 of regression coefficients, dataset of 8 varying parameters of the bracing ($\sigma = 0.2$) | 59 |
| 4 | Quadratic terms \mathcal{B}_2 of regression coefficients, dataset of 8 varying parameters of the bracing ($\sigma = 0.2$) | 59 |

Nomenclature

All dimensions and coordinates are expressed in mm, all angles are expressed in radians.

Auxiliary Parameters

- α_K angle between the V braces and the outermost fan brace in the reference model
- α_{out} angle of the outermost brace in the fan layout
- n_b number of braces in the lower bout
- n_{fan} number of braces in fan configuration
- V total volume of the braces in the lower bout

Parameters of the Bracing

- α_V angle between the lower (V) braces and the x axis
- α_{fan} parameter that defines the fan bracing angle
- h_{max} maximum thickness of the braces, or thickness at the center of their curved profile
- h_{min} minimum thickness of the braces, or thickness at the edges
- l_V length of the lower (V) braces
- s scalloping factor of the braces
- w width of the braces
- y_V y -coordinate of the center of the V braces

Parameters of the Outline

- $c_{n,x}$ x -coordinate of the center of circle n where $n \in [1, 4]$ refers to one of the circles defining the outline
- $c_{n,y}$ y -coordinate of the center of circle n
- r_n radius of circle n
- w_1 width of the flat part in the lower bout
- w_2 width of the flat part in the upper bout

1

Introduction

1.1 Aim of the Thesis

Classical guitar is a musical instrument finely crafted by luthiers who carry on secular traditions. Although the definition of a modern guitar originates in the work of Spanish luthier Antonio de Torres in the middle of the 19th century, many innovations regarding the soundboard and bracing layouts have been brought during the 20th century. Technological development and the interest of companies have been encouraging an engineering approach to musical instrument making to complement the artisan one. The interest in knowing the vibrational character of stringed instruments has multiple goals. The research of alternative materials [4, 5] to substitute increasingly rare or expensive ones, the implementation of physical models of sound generation, the optimization of the tonal quality and radiation efficiency are some of the most relevant examples of the interests behind the study of the acoustics of guitars and musical instruments in general.

Although the working principles of the instrument are rather simple if we try to broadly picture the instrument as a system of coupled vibrators with a resonator [6, 7], a complete and detailed tonal characterization of a guitar would be definitely complex. Many components actually interact with each other and contribute to the sound of the instrument, therefore we are still not able to address the role of each one of the luthier's building choices to define a completely engineered model.

For this reason research proceeds in very focused ways to answer the many specific questions that can be roughly summarized with: "how is guitar sound characterized by its components?".

Our goal is to find numerical models to predict the natural frequencies (also called eigenfrequencies) of the braced soundboard from its geometrical features. The analysis of the natural frequencies gives important information about the tone color of the complete instrument. We stick to the most traditional guitar model, considering the outline of the Torres guitar with fan bracing and analyzing the effect of small variations of the geometry and the number of braces in the fan layout.

This work fits in the research area of guitar modal analysis, specifically on the soundboard vibration alongside studies focused on the effect of classical guitar bridge [8], on the difference between bracing layouts [9, 2], on the effect of adding elements in the fan layout [10] or changing the position of a single brace [11]. Furthermore, the effect of scalloped braces has been measured on rectangular panels [12].

All of these studies measure the impact of various elements on the natural frequencies of the soundboard because it is the main acoustic radiator of the instrument and it is the component that most affects the sound of the complete instrument.

Some models even manage to approximate the resonances of the full instrument knowing the eigenfrequencies of the soundboard and the geometry of the full instrument [7].

Even if many study cases have been already successfully covered, we are still not ready to describe entirely the vibratory behavior of the guitar based on its geometrical representation and its material specifications without building it or performing a numerical simulation.

To model the eigenfrequencies of different soundboards we perform Finite Element Modal Analysis on their meshes, a type of numerical simulation that calculates the normal modes of physical systems.

This method has been validated on full guitars [13, 14], guitar bodies [9, 2] and piano soundboards [15], performing experimental modal analysis on real copies of the meshes with reliable results.

Usually, guitars are studied with a fixed boundary condition to mimic the working conditions of the complete instrument and the test setup of luthiers which measure the soundboard in the mold [7], so we used the same condition for our simulations.

The results of our simulations are used to build a regression model that predicts the eigenfrequencies of the soundboard from a set of geometrical parameters that describe its shape and its bracing system.

Our model considers all the parameters simultaneously in order to account for the combined contributions, accurately predicting the eigenfrequencies.

1.2 Application Fields

The relationships between geometric parameters and natural frequencies of the soundboard of a guitar are useful indications for the design of an instrument, whether performed by a luthier or in an engineered process. Each influent parameter is a degree of freedom for the control of the tone, allowing a wide range of possibilities to operate an adjustment of the frequency response.

Although this work is focused on a very specific type of instrument, the outline of classical guitars is almost standard, and the relations we measured between its dimensions and its vibrational behavior can be taken into account with the right amount of care for guitars with different bracing systems.

The proposed methodology is valid for the analysis of the vibration of musical instruments in general, but also for any kind of modal analysis of complex shapes where is necessary to control the natural frequencies during design. This situation is common in structural engineering problems where the normal modes of a solid can cause excessive vibration or a collapse.

1.3 Thesis Outline

This thesis is composed of three main parts.

After this introduction, Chapter 2 covers the background on the classical guitar and the state of the art on the vibratory analysis of its soundboard from different perspectives. The theoretical background on the Finite Element Method and its software implementation are also discussed.

In Chapter 3 we describe the methodology we adopted to build a parametric model of a guitar shape that can be used to generate a dataset of different meshes.

In Chapter 4 we describe the modal analysis of the dataset of soundboards starting from the configuration of the simulations. We organize the results of the simulations classifying the eigenfrequencies with respect to the corresponding modal shape in order to compare the same mode for all the samples.

Then we present a regression analysis on the results of the simulations to predict the eigenfrequencies from the geometrical features for a fully parametric shape and a study case dedicated to braces only.

Finally, we draw the conclusions in Chapter 5 and discuss possible future research works on the topic.

2

State of the Art and Background

In this chapter, we go through the topics that are introductory for our study to properly understand the subject and its context.

We start by describing the instrument that is at the center of the thesis, the classical guitar; we present a quick overview of its components and their working principles with some historical context. We go more in-depth about the soundboard and the bracing describing some of the choices that guitar makers do when they design and build their instruments.

In the second part, we present the most relevant methods used to find which are the modal shapes and eigenfrequencies of soundboards of violins and guitars. We show that luthiers and researchers have different approaches and tools to study musical instruments but eventually their results can converge and build important shared knowledge.

Among the methods presented in the second part, the FEM method is the one that we adopted for our study: theoretical background on this topic is given in the third part of this chapter. The practical steps we performed to configure the software for our simulations are described in section 4.1.

2.1 The Classical Guitar and its Components

Classical guitar is a plucked string instrument of the lute family. Its strings are mainly tuned by fourths with the standard tuning being E4, B3, G3, D3, A2, E2. The strings are parallel to the instrument and extend from the peghead or headstock to the bridge placed in the middle of the soundboard. The resonator of the instrument is its body, composed of a backplate, a front plate with an opening called soundhole, and enclosed by the sides.

The body of the guitar has a characteristic outline that identifies three main areas: from the tailpiece to the neck joint we have the lower bout, the waist and the upper bout. The neck is attached to the body by means of the neck joint or heel and its front surface is glued to the fretted fingerboard. An overview of the guitar parts is visible in figure 2.1.

The dimensions of the guitar are not strictly defined, full-sized instruments have a scale length of 650 mm circa referring to the distance from the bridge saddle to the nut. Baritone and bass guitars as well as various short-scale instruments are made, with the overall dimension of the instrument adapted according to the scale [16].

The modern guitar shape derives from the instruments of Antonio de Torres, one of the most important luthiers in history whose guitar-making tradition spread from southern Spain in the late 1800s influencing what is now worldwide conceived as classical guitar. Torres guitars have a shape that is very similar to the modern concert guitar also in terms of dimensions with the body being approximately 368 mm wide at the lower bout and 490 mm long.

Classical guitar soundboards are usually composed of two symmetric pieces of quarter-sawn spruce or cedar, glued in the centerline that runs from the tailpiece to the neck joint. The sides and the backplate are made of a different wood, usually rosewood, maple or fruitwoods. The back is built gluing two or more plates of wood like the top plate, but it is more arched and its bracing system is usually composed of transverse braces only. Its thickness is about 2 mm.

The most important component for what concerns the tone of the instrument is the soundboard, its material and bracing system are chosen by the luthier to achieve the desired sound. For this reason, soundboards are usually the parts of stringed instruments that require the most valuable pieces of wood and to which many measurements and tuning procedures are performed.

We now go in-depth describing the elements that are most involved in the guitar tone.

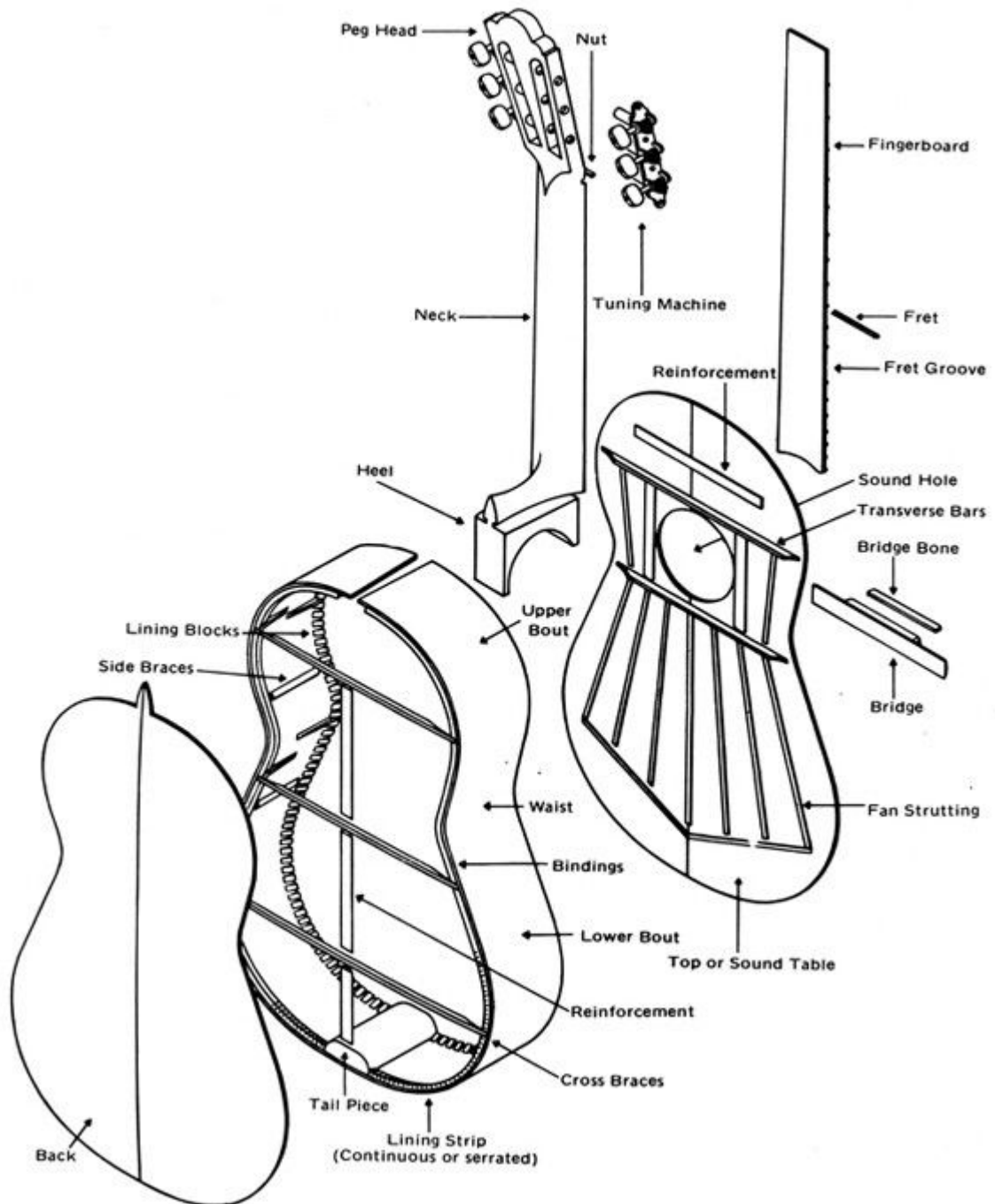


Figure 2.1: Exploded view of a classical guitar [1].

2.1.1 The Strings

The excitation that is responsible for the sound of the guitar is applied to the strings by the player's fingers. The technique of the player, as well as the string plucking point and material, are the first of many factors that influence the resulting sound [17, 18].

While the first guitars were equipped with strings made of gut, modern guitars come with nylon strings. Usually, the three thicker strings are wound to increase their mass per unit length. In this way, they reach lower frequencies with tension and size of the section that are comfortable for the player. In fact, the length of the vibrating portion of the string, its mass and its tension determine the pitch of the played note. The fundamental frequency f_f of a string can be calculated as

$$f_f = \frac{1}{2L} \sqrt{\frac{T}{\mu}} \quad (2.1)$$

where the string properties are represented by its length L and its mass per unit length μ while the tension is indicated with T .

The peg head holds the strings by means of the machine heads that allow to adjust the string tension and tuning, using rotating knobs. The other end of the string is tied to the bridge.

2.1.2 The Bridge

The vibration of the strings is transmitted to the instrument in the two endpoints of their vibrating length. Most of the energy transmitted to the soundboard travels through the bridge, in particular the saddle (called bridge bone in figure 2.1), and makes it move. The bridge is therefore important for the coupling between the string and the soundboard for the propagation of the vibration.

Since the string is free to move in the infinite planes that cross its resting position, the force exerted on the bridge by the vibrating motion has a variable direction. Consequently, the bridge exhibits a composite motion: a rocking motion due to the string vibration parallel to the bridge and a motion towards the body due to the string motion in the same direction [6].

In correspondence with the bridge position, on the internal side of the soundboard an additional wood plate can be present to reinforce the joint. Both the bridge and the underlying plate add mass and stiffness to the central region of the soundboard, so their dimensions affect the instrument resonances [8].

2.1.3 The Soundboard

The soundboard (or top plate) is a common element between all the stringed instruments, it is as simple as essential for the characterization of the tonal quality and the acoustic radiation.

In classical guitars, the soundboard is a plate of wood usually spruce or cedar with a soundhole in the upper part, between the transverse bars. Its thickness can vary from 1.5 to 3 mm depending on the material, the arching and the bracing system, parameters that are chosen coherently by luthiers to account both for tonal characteristics and structural strength. The sides and the plate are joined by the linings, a structure that increases the surface to which the soundboard is fixed along the whole outline. Through the linings, the boundary condition for the vibration of the top plate changes from the ideal simply supported edge to a clamped edge condition, meaning that few millimeters from the outline inwards are not free to move. The size of the linings and the presence of carvings on them called kerfs, hamper to different degrees the vibration of the outer part of the surface.

The vibration of the soundboard causes both sound radiation outside the instrument and an inward pressure wave. The resonances of the air inside the guitar and those of the front and back plates characterize the frequency response of the instrument. This is more evident at low frequencies for which basic models have been developed to describe the sound generation of the guitar with a system of a few elastic parts and a Helmholtz resonator [7, 6]. The response at higher frequencies is more involving the vibration of the soundboard which is therefore functional to the brilliance of the instrument.

2.1.4 The Bracing

The tonal quality of the soundboard is affected by the underlying bracing system. Thick soundboards with transverse braces were originally employed to resist the pull of the strings that exert a total tension of about 47 kg.

In the late 1800s, the demand for louder instruments drove the spread of guitars with thinner soundboards that radiate more power, compensating the weaker structure with additional thin braces made of the same material as the top plate and removing the transverse braces in the lower bout.

It was in this period that the Spanish guitar-making tradition began to spread, gradually leading to the use of the geometry of the Torres guitar and the fan-shaped bracing system.

The fan layout consists of a set of thin braces developing from the transverse strut under the soundhole to the lower edge of the guitar where two additional braces can be placed in a v-shape enclosing the fan figure like in figure 2.1.

These braces are glued to the soundboard after the bridge plate and lie



Figure 2.2: Different bracing systems for classical guitars. From left to right: Torres, lattice, Kasha and radial.

above it.

Many other building styles are used nowadays, some examples are shown in figure 2.2; it is worth mentioning the X-shaped bracing developed by Martin in the 1850s which is also widely employed on steel-string acoustic guitars, the radial layout in which the braces are placed around the bridge with radial orientation, the lattice layout employing two crossed sets of parallel thin braces, the Kasha asymmetric bracing, and the double-top guitars which soundboard is made by a thin honeycomb synthetic layer enclosed by two wood plates [19].

Different bracing styles aim to different goals such as loudness, brilliance, sustain, and tone. Although research has proven some objective differences between bracing systems [9, 2, 20], a perfect instrument does not exist and the choice of its features ends up being a trade-off that takes into account also the musical context of its performance and the subjective personal taste.

The cross-section of the braces is usually rectangular or rounded and their thickness is not uniform. After they have been glued to the soundboard, luthiers carve the struts to remove mass from the soundboard and tune its resonances to specific frequencies. Since the vibration near the outline is hampered by the linings, braces are usually scalloped in that area to keep the vibrating area as large as possible.

2.2 State of the Art on Modal Analysis of String Instruments

The modal analysis of a resonant system consists of the study of its dynamic properties in the frequency domain. When analyzing a resonant component of a musical instrument, vibrations at different frequencies are usually measured in the steady-state condition. The most important frequencies in musical instruments are the eigenfrequencies (or natural frequencies) of their normal modes because they correspond to the maxima of the frequency response.

The normal modes of soundboards have been studied for centuries thanks to the characteristic vibration shapes that they assume along the surface called modal shapes.

Violin and guitar plates are studied in a slightly different setting: while violin plates are tuned in the carving stage by regulating the thickness profile, guitar soundboards are measured just before the braces are added. The braces add stiffness that raises the eigenfrequencies of the plate depending on their height and profile [12], therefore the luthier proceeds carving the braces to achieve the desired tone. The goal of this stage is to have a proper value of the eigenfrequencies and a reasonable ratio between surface and mass of the vibrating area [7].

When measuring the vibrational behavior of a plate it is important to accurately control its boundary conditions. Both the free and the clamped boundary conditions are used: for the free condition, the plate is usually suspended with a system of elastic bands, while the clamped one can be realized with a mold.

Nowadays, luthiers still rely on approximate methods to tune the top plate of violins and guitars. The traditional techniques used to measure the eigenfrequencies of the plates are the *tap-tone* method and the Chladni patterns [21].

In the context of industrial and academic research, the Chladni patterns are commonly considered, but also more advanced methods have been developed with the help of software simulations and electronic measuring instruments.

We now describe the main methods employed for the analysis of the resonances of the soundboards.

The Chladni Pattern method is used to find the eigenfrequencies of the soundboards and visualize the corresponding modal shapes.

The procedure involves dust or sand being scattered over the surface of a plate lying in horizontal position. When one of the resonances of the plate is excited the particles jump across the surface and tend to collect along the nodal lines. If the mode is excited for enough time and with enough energy, the nodal lines become visible where the powder is concentrated and the lobes of the vibration correspond to the uncovered areas.

The original method of excitation was to run a bow on the plate edge until a vibration mode was excited. From the 20th century, loudspeakers were employed for easier and more precise control of the frequency of the excitation: if a sufficiently powerful speaker is placed under a suspended plate, the emission of a pure tone by the speaker is able to excite the corresponding resonance of the plate. Another possible method of excitation is the use of a shaker as shown in figure 2.3.

A non-invasive method for the visualization of the vibration modes is given by the holographic interferometry [2, 22, 23]: with this method, the vibration of the structure can be detected without even touching it.

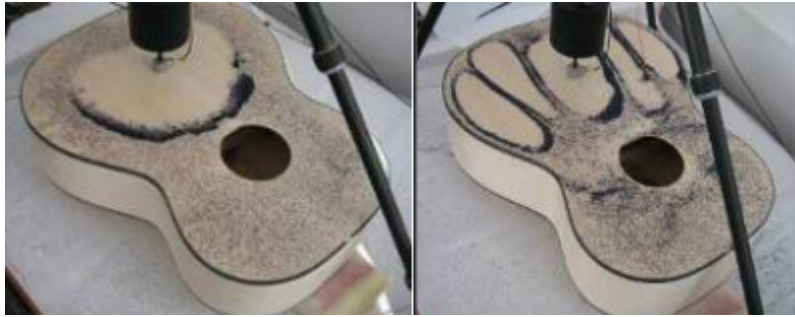


Figure 2.3: Chladni patterns of a soundboard mounted on a guitar body, excited at two different frequencies [2]

The tap-tone technique is another method used to find the eigenfrequencies of a plate but in this case, it is more convenient for the luthier to know approximately the nodal lines of the modes he is analyzing.

To measure the eigenfrequency of a mode, the luthier holds the plate with two fingers in a nodal position and taps it in the middle of an antinodal position. The luthier holds the plate close to his ear to listen to the resulting tone. The sound is percussive and quickly decaying, so the individuation of the frequency is quite difficult and not precise.

Nodes and antinodes of the resonances can be found repeating this method with different tap positions and the same hold position or vice versa. Marking the still zones of the plate for many measurements allows identifying the nodal lines, while the unmarked surfaces correspond to the vibration lobes.

The FRF method gives a complete frequency response of a resonant object computing the transfer function between a controlled excitation signal and a response signal acquired through a sensor.

The excitation signal can be generated through an impact hammer that also records the force applied during the measurement. The hammer excitation generates an impulsive signal that carries energy across a range of frequencies depending on the hardness of the hammer tip. Soundboards of various instruments like guitars [24], violins [25] and pianos [15] have been studied with this method: accelerometers are positioned on the soundboard in a non-symmetric location with respect to the excitation point to record the plate response. The hammer and accelerometer signals are simultaneously acquired and a transfer function is calculated from the acquired data.

The FRF method provides the point-to-point frequency response for an entire frequency band defined by the acquisition system properties. Since we are interested in studying the vibrational behavior of the full plate, the measurement has to be repeated at various points of the surface through the roving hammer technique or the roving accelerometer one. The results can be interpolated across the surface to get the frequency response of the whole plate.

The FEM simulation is a software-powered technique that computes the normal modes of an object analyzing its geometrical representation. The object is represented by a mesh of points that divide its volume into small elements like for example tetrahedrons called finite elements.

The FEM simulation solves the equations of motion that describe the normal modes of the geometry in all the points, providing its modal shapes and eigenfrequencies. The frequency response function and the transient response can also be calculated with this method using different settings for the solver.

The mesh can be created with CAD software or generated with the 3D scan of a real object. We used a third way for our analysis and realized a Matlab script that creates a mesh of a guitar soundboard given its geometrical parameters.

The FEM is a powerful tool but it operates on virtual representations which are just approximations of the real plate. For this reason, they are used to model the behavior of a class of instruments rather than properly predict the result of a given sample, although the result can in many cases be very accurate. FRF method can be used to validate the results obtained through FEM simulations, comparison between these two methods for guitar bodies has been presented in [9] and [2]. More details on the FEM are given in the next section.

2.3 Background on Finite Element Method

Space- and time-dependent physical problems are generally expressed by partial differential equations (PDEs) that can be solved analytically only for simple shapes [3].

Most of the stringed instruments have soundboards with irregular shapes for which the PDEs that describe the vibration of the surface need to be simplified. In particular we are interested in computing the wave equation:

$$\nabla^2 u = \frac{1}{c^2} \frac{\partial^2 u}{\partial t^2} \quad (2.2)$$

where $\nabla^2 = (\frac{\partial^2}{\partial x^2}, \frac{\partial^2}{\partial y^2}, \frac{\partial^2}{\partial z^2})$ is the Laplace operator in the three dimensions x, y, z . The wave propagation speed of the material is indicated by c , and $u = u(x, y, z, t)$ is the displacement of the soundboard from its resting position.

With the FEM we compute an approximated numerical solution of the PDEs in the discretized space. The problem is simplified as a system of Ordinary Differential Equations (ODEs) for which the solution is calculated in each point of the mesh, forming a piecewise approximation of the real solution.

2.3.1 Theoretical Background on FEM

The FEM begins with an ordered and well defined series of steps to transpose a physical problem into a computable numerical approximation. Considering for simplicity a one dimensional wave propagation problem

$$\frac{\partial^2 u(x, t)}{\partial t^2} - c^2 \frac{\partial^2 u(x, t)}{\partial x^2} = f(x, t) \quad (2.3)$$

FEM requires it to be defined in an integral form called *weak formulation* [26]

$$\int_{\Omega} \frac{\partial^2 u(x, t)}{\partial t^2} v(x, t) dx - \int_{\Omega} c^2 \frac{\partial^2 u(x, t)}{\partial x^2} v(x, t) dx = \int_{\Omega} f(x, t) v(x, t) dx \quad (2.4)$$

where Ω is the domain in which the function is evaluated and $v(x, t)$ is a test function. The functions u and v are assumed to belong to the Hilbert space $H^1(\Omega) = \{u, v : \Omega \rightarrow \mathbb{R} | v, v', u, u' \in L^2(\Omega)\}$, with L^2 indicating the Lebesgue space to guarantee that the integrals assume finite values. This formulation accompanied by the aforementioned assumption and boundary conditions represents a well-posed problem that can be solved in the finite element space.

The discretization of the domain Ω is achieved defining a basis like shown in figure 2.4. This formulation in the discretized domain can be properly expressed using an approximated variable $u_h \approx u$ as

$$u_h = \sum_i u_i \psi_i \quad (2.5)$$

where ψ_i indicates the i -th basis function in the domain Ω .

The problem 2.4 can be projected in the discretized space using the Galerkin formulation as

$$\int_{\Omega} \frac{\partial^2 u_h(x, t)}{\partial t^2} v_h(x, t) dx - \int_{\Omega} c^2 \frac{\partial^2 u_h(x, t)}{\partial x^2} v_h(x, t) dx = \int_{\Omega} f(x, t) v_h(x, t) dx \quad (2.6)$$

Equation 2.6 can be expressed in a second order ODE with coefficients arranged in matrices to allow its algorithmic computation in all the finite elements of the mesh

$$\mathcal{M} \frac{\partial^2 u_h(x, t)}{\partial t^2} + \mathcal{A} u_h(x, t) = \mathcal{F}(t) \quad (2.7)$$

with the matrices defined as

$$\mathcal{M}_{ij} = \int_{\Omega} \psi_i \psi_j dx \quad \mathcal{A}_{ij} = c^2 \int_{\Omega} \frac{\partial \psi_i}{\partial x} \frac{\partial \psi_j}{\partial x} dx$$

$$\mathcal{F}(t) = \left(\int_{\Omega} f \psi_1 dx \quad , \dots, \quad \int_{\Omega} f \psi_j dx \right)^t$$

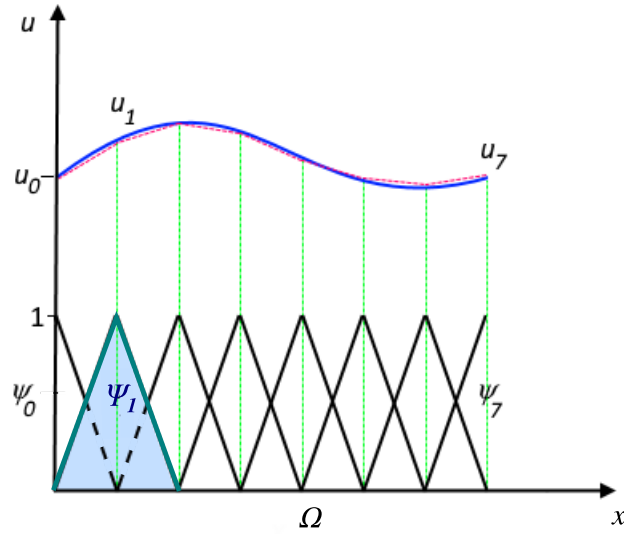


Figure 2.4: The function u (solid blue line) is approximated with u_h (dashed red line), which is a linear combination of partially overlapping piecewise linear basis functions ψ_i indicated in black (the shape of a single contribution ψ_1 as an example is represented by the cyan triangle). The coefficients are denoted by u_0 through u_7 . [3]

The last step to obtain a fully computable problem is time discretization. To solve 2.7, each matrix element has to be computed at each time interval with a time-marching scheme. The time derivatives need to be approximated, for example using finite differences for a time step ΔT as

$$\frac{\partial u_h(x, t)}{\partial t} \approx \frac{u_h(x, t + \Delta t) - u_h(x, t)}{\Delta t} \quad (2.8)$$

In modern software, the time intervals and stepping schemes are automatically handled across the simulation steps to optimize the computation while respecting the convergence conditions [3].

The solution for a one-dimensional wave propagation problem consists of a series of snapshots of the displacement across time. A visual representation can be generated by software evaluating the displacement of each point of the mesh and presenting an animation or a plot of the temporal evolution of the system.

2.3.2 The Finite Element Modal Analysis

Since we deal with a solid, the one dimensional wave equation is not enough to represent wave propagation in the soundboard. The type of material under analysis defines the governing equation of motion of its finite elements. For a *linear elastic material*, the relation between stresses

and strains is expressed by Hooke's law [27]

$$\boldsymbol{\sigma} = \boldsymbol{\sigma}_{ex} + \mathcal{C} : (\boldsymbol{\epsilon} - \boldsymbol{\epsilon}_{inel}) \quad (2.9)$$

where $\boldsymbol{\sigma}_{ex}$ represents the contribution of the initial and viscoelastic stresses, \mathcal{C} is the 4th order elasticity tensor, the symbol ":" indicates the double-dot tensor product or double contraction, and $(\boldsymbol{\epsilon} - \boldsymbol{\epsilon}_{inel})$ is the elastic strain tensor expressed as the difference between the total and the inelastic components. The stress tensor $\boldsymbol{\sigma}$ can be represented in matrix form as

$$\boldsymbol{\sigma} = \begin{bmatrix} \sigma_x & \sigma_{xy} & \sigma_{xz} \\ \sigma_{xy} & \sigma_y & \sigma_{yz} \\ \sigma_{xz} & \sigma_{yz} & \sigma_z \end{bmatrix} \quad (2.10)$$

where the two pedices of the elements indicate the direction of the force application and the normal to the surface to which the force is applied. The tensor is symmetric and represented by a total of six independent variables. The same representation holds for the strains $\boldsymbol{\epsilon}$. Stresses participate to the force balance in Newton's second law as

$$\nabla \cdot \boldsymbol{\sigma} + \mathbf{f} = \rho \frac{\partial^2 \mathbf{u}}{\partial t^2} \quad (2.11)$$

where $\nabla \cdot \boldsymbol{\sigma}$ is the three dimensional gradient of the stress tensor, \mathbf{f} is the force per unit volume applied to the system, ρ is the material density and \mathbf{u} is the displacement vector.

The type of material determines the expression of the stress terms. For orthotropic materials like wood, the Hooke's law can be expressed in matrix form as

$$\begin{bmatrix} \sigma_x \\ \sigma_y \\ \sigma_z \\ \sigma_{xy} \\ \sigma_{yz} \\ \sigma_{xz} \end{bmatrix} = \begin{bmatrix} \sigma_x \\ \sigma_y \\ \sigma_z \\ \sigma_{xy} \\ \sigma_{yz} \\ \sigma_{xz} \end{bmatrix}_{ex} + \mathcal{D}^{-1} \left(\begin{bmatrix} \epsilon_x \\ \epsilon_y \\ \epsilon_z \\ 2\epsilon_{xy} \\ 2\epsilon_{yz} \\ 2\epsilon_{xz} \end{bmatrix} - \begin{bmatrix} \epsilon_x \\ \epsilon_y \\ \epsilon_z \\ 2\epsilon_{xy} \\ 2\epsilon_{yz} \\ 2\epsilon_{xz} \end{bmatrix}_{inel} \right) \quad (2.12)$$

where \mathcal{D} is the symmetric compliance matrix, composed of the elastic parameters of the material: the Young modulus E , the shear modulus G

and the Poisson ratio ν .

$$\mathcal{D} = \begin{bmatrix} 1 & -\frac{\nu_{yx}}{E_x} & -\frac{\nu_{zx}}{E_z} & 0 & 0 & 0 \\ \frac{\nu_{xy}}{E_x} & 1 & -\frac{\nu_{zy}}{E_z} & 0 & 0 & 0 \\ -\frac{\nu_{xz}}{E_x} & -\frac{\nu_{yz}}{E_y} & 1 & 0 & 0 & 0 \\ 0 & 0 & 0 & \frac{1}{G_{xy}} & 0 & 0 \\ 0 & 0 & 0 & 0 & \frac{1}{G_{yz}} & 0 \\ 0 & 0 & 0 & 0 & 0 & \frac{1}{G_{xz}} \end{bmatrix} \quad (2.13)$$

The combination of inertia and elasticity, through Newton's second law 2.11, gives the Navier-Stokes equation for elastic solids whose solutions are wave-type functions [28]. Applying boundary conditions and assuming a harmonic solution, this system translates into an eigenvalue problem whose solutions are the natural frequencies.

2.4 Concluding Remarks

A deep study of classical guitar tone is a complex topic that involves different approaches to analyze the factors that participate in the sound generation. In this chapter we presented the necessary background to understand the purpose of the modal analysis of a guitar soundboard, its theoretical foundations and the state of the art from different points of view.

At first, we showed that the classical guitar is a quite complex instrument that has undergone major development during the last two centuries concerning both the bracing layout and the soundboard. Then we discussed the main tools and techniques that are used to infer the resonances of the plates from the point of view of both the luthier and the engineer.

We finally introduced the theoretical background on the Finite Element Modal Analysis, showing the main equations and parameters that characterize these tools.

3

Building a Parametric Mesh of a Braced Guitar Soundboard

In this chapter, we describe the process through which we created sample meshes of guitar soundboards. The goal is to obtain a variety of samples with different geometries, which we can be able to analyze with the Finite Element Method.

We have chosen the Torres guitar as a reference model to generate the dataset, so we replicated its outline starting from simple shapes and superimposed the result to a picture of a real guitar to check the accuracy of the replica.

From the shape of the replica, we derived a set of parameters that describe the full geometry and are suitable for the generation of other guitar shapes. The parameters concern the guitar outline, the bracing layout, and the dimensions of the braces. The variety of the created samples comes from the modification of such parameters in a random way.

We created the meshes by first defining the points of the outline and soundhole and then placing the internal points to create the plate. The meshes of the braces are built so that they adhere perfectly to the soundboard, to allow the union of all the elements in a single mesh on which our analysis is performed.

3.1 Definition of the Geometrical Parameters

Today's guitars are an extremely common instrument with a characteristic shape, easily recognizable by everyone. To synthesize a guitar plate, we have chosen as a reference instrument the Torres guitar that is one of the most influential models in the classical guitar tradition. Its body is a model for the shape of guitars from the mid-nineteenth century, so we used pictures of this instrument and schemes of its geometry to replicate both the outline and the braces.

3.1.1 Outline Parameters

The shape of guitars [29], as well as many stringed instruments [30], has been traditionally defined using circular shapes related by harmonic dimensions like simple fractions and golden ratios. The number and the layout of the circles is not constant when characterizing a type of instrument like the guitar throughout its evolution, but some features have remained almost unchanged since well before the Torres era. As visible in figure 3.1, the contour of a guitar plate is characterized by three main curves that identify three main areas of the guitar body: the upper bout, the waist, and the lower bout.

Our process of building a model of a guitar starts from the definition of these three curves, which we found well represented by three properly positioned circles. The outline is not an entirely curved shape though, guitar bodies are often built with flattened edges behind the neck and in the tailpiece.

The first step to create the model is to get a continuous line from the connection of the circumferences. We constrained the line to overlap to three arcs of the circumferences and defined two couples of points that flatten the curve at the edges. We got the full contour simply mirroring the described half with respect to the y axis.

The other characteristic shape that defines the guitar body is the soundhole, also represented by a circle.

Positioning these circles and points correctly, we have been able to get an outline that is visually well superimposed to a picture of a real guitar.

In figure 3.1 on the left the construction of the outline using three circles is shown: the characterizing circles are shown in blue, where the thicker lines represent the arcs in which they are perfectly superimposed to the outline. Two flattened lines are present also in the upper and lower edges of the outline. On the right, the result of the correct arrangement of the circles is shown: the dashed lines superimposed to the picture represent the reconstructed outline and soundhole. To get a uniform distribution of points in the outline, we applied a Matlab interpolation algorithm [31] that creates a curve passing through the defined points



Figure 3.1: Definition of the outline. In the left image the thick blue lines represent the constraints on which the outline overlaps. The dashed lines in the right image represent the resulting outline and soundhole.

using natural cubic spline functions [32].

Once the shape was correctly superimposed to the reference figure, we parametrized the geometry through the radii and positions of the centers of the circles used to shape the outline. Since the parameters are intended to vary in a range that is proportional to their reference value, we have chosen them to give the outline a proportionate variation in all its dimensions. For this reason, we express the coordinates of the three outline circles as their distance to the centerlines of the guitar body. The parameters of the outline are indicated in figure 3.2: the three circles that define the outline are controlled by the positions of their centers c_1, c_2, c_3 and their radii r_1, r_2, r_3 . With w_1 and w_2 we indicate the width of the flattened parts of the outline in the lower bout and upper bout respectively.

The waist should undergo only a little variation to avoid the outline being distorted, so it has fewer parameters and smaller values than the bouts circles. The horizontal position x_2 of the waist circle is a function of the other outline parameters: we keep it at a constant distance dx_2 from the line connecting the centers of the two bouts circles $c_1 = (x_1, y_1)$ and $c_3 = (x_3, y_3)$

$$x_2 = \frac{y_2 - q_{1,3}}{m_{1,3}} - dx_2 \quad (3.1)$$

where $m_{1,3}$ and $q_{1,3}$ define the equation of the line connecting the two

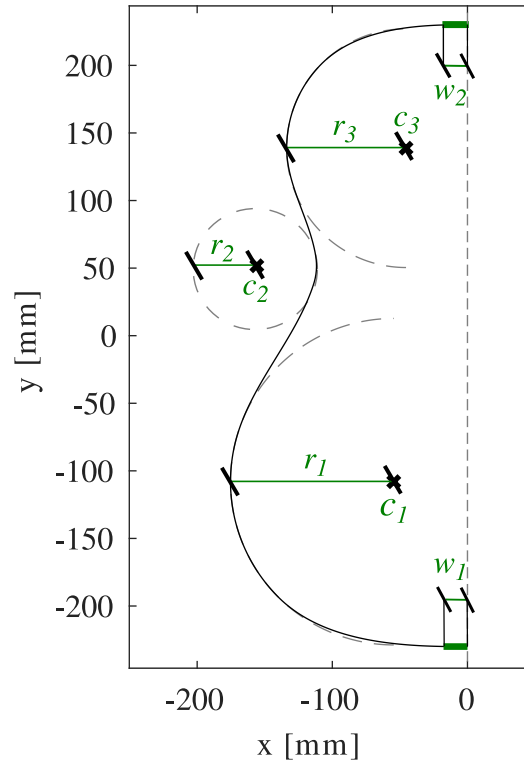


Figure 3.2: Outline parametrization. The variable parameters are indicated in green, the constant parameter is indicated in red. The y axis is highlighted with a black dashed line and constitutes an axis of symmetry for the soundboard.

circles as

$$y = m_{1,3}x + q_{1,3} = \frac{y_3 - y_1}{x_3 - x_1}x + y_3 - \frac{y_3 - y_1}{x_3 - x_1}x_3 \quad (3.2)$$

in this way, the depth of the waist curve is dependent only on the radius of the middle circle.

For the soundhole, we have taken as variable parameters the radius and the y -coordinate of the circle center, while its x -coordinate is set to zero to maintain the symmetry.

3.1.2 Bracing parameters

Classical guitars have typically thicker braces in the upper half for structural support and a thinner bracing layout in the lower bout on which luthiers operate to control the tone color and radiation power of the instrument: for this reason we define variable parameters only for the lower bout braces.

The bracing configuration we considered is also inspired by the Torres guitar but compared to the body shape, the bracing layouts are less standard. To build our model, we referred to the scheme of a guitar with three

horizontal structural braces and two thin wood plates near the soundhole. In the lower bout, we use the fan pattern that is employed in the original Torres model. Many other configurations are actually common for the lower bout bracing, but we stick to the more standard case. The reference layout has five braces in fan configuration and two braces placed in a v shape below the fan layout. An overview of the bracing layout and the thickness of the assembled geometry is visible in figure 3.3. Looking at the thickness profile of the soundboard is possible to sense the position and dimension of the braces: dark blue indicates the constant thickness of the plate, light blue indicates the thin braces, and red highlights the thicker section of the transverse braces.

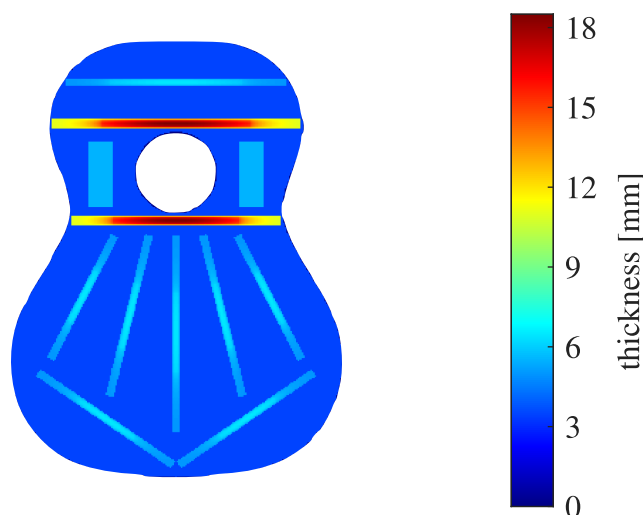


Figure 3.3: Thickness of the reference soundboard with bracing

Each brace consists of a bar of wood glued to the soundboard by a perfectly adherent rectangular face. The opposite face is curved, with the maximum thickness at the center of the brace, like shown in figure 3.4. We do not consider different sections, hollow braces or different types of cuts.

Scalloping is also applied to the braces, furtherly reducing the thickness at the edges.

The only exception in the braces shaping are the two thin plates near the soundhole, that have a constant thickness without curvature or scalloping.

From the reference model, we take as parameters of the braces the width of their cross-section w , the thickness at the edges h_{\min} , and the thickness at the center h_{\max} . We control the length of the scalloped parts of the brace with the coefficient s . The values of s are defined in the range 0 to 0.5: the extreme values correspond to no scalloping and edges scalloped until the middle point respectively.

Since in the reference scheme all the braces in the lower bout have the

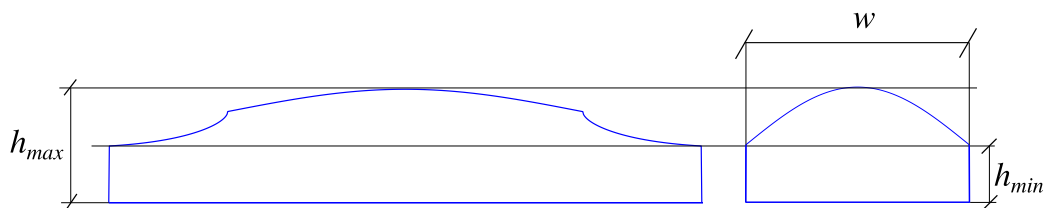


Figure 3.4: Orthogonal views of a brace shape: longitudinal view on the left and cross-section on the right. The surface of contact with the plate is shown flat but actually follows the light curvature of the soundboard. The parameters h_{\min} and h_{\max} define the thickness of the brace at different points and w defines its width.

same cross-section, we considered a single occurrence of the aforementioned parameters as controlling each brace in the lower bout collectively.

Also concerning the bracing layout, we have chosen the parameters to control angles and locations of multiple elements with single values. From the position of the lower braces and the angle of the outermost fan brace, we reconstruct the positions of all the braces positioned internally in the fan shape. The layout we used is always symmetric, so we defined the parameters to describe one half of the geometry that can be mirrored with respect to the y axis as done for the outline.

The y -coordinate of the two lower braces y_V refers to the absolute position of their centers; the angle α_V indicates the angle between the lower braces and the x -axis: with these two parameters we can define a line equation that sets a lower boundary for the extension of the fan braces, which are set to extend until a few millimeters from the lower braces. The length of the two lower braces l_V is also variable but does not affect the fan bracing at all.

The angles of the fan braces depend on a single parameter called α_{fan} that linearly distributes the angle of each element in a range $[\alpha_{\text{out}}, \pi - \alpha_{\text{out}}]$ where the angle of the outermost brace is defined as

$$\alpha_{\text{out}} = -\alpha_{\text{fan}} + \alpha_K \quad (3.3)$$

The angle α_K is defined as the angle formed by the lying lines of the lower and outermost fan braces in the reference 5 braces model as showed in figure 3.5. The value of α_{fan} does not refer directly to any geometrical entity, but its mean value is equal to the one of α_V . In this way, the variation of the angle of the lower braces and the fan braces are in a comparable range.

Through this kind of parametrization, we can manage any number of braces in the fan layout.

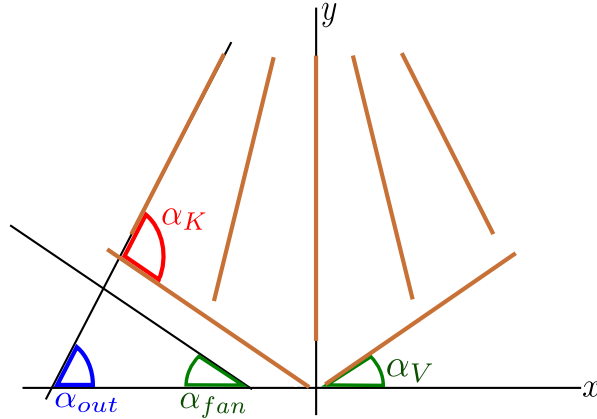


Figure 3.5: The bracing orientations are driven by two independent angles, depicted in green. The angle α_K is a constant term to get the angle of the outermost fan α_{out} from the parameter α_{fan}

3.1.3 From the Torres Reference Model to a Dataset of Guitar Plates

In the previous sections, we described the geometry we are treating and the 20 geometrical parameters that allowed us to generate many variants of the reference model. We summarize the parameter names and meaning in table 3.1. We recall that any coordinate and length value is expressed in mm and any angle is expressed in radians.

Although the elements we defined can depend on each other in shape or position, we have chosen each one of these 20 parameters to be independent of the others 19. Each dependent feature like the position of the waist circle or the length of the fan braces is expressed by a rule depending only on this set of parameters, as we will specify in the next sections.

We analyzed also a second dataset to inspect more accurately the influence of the braces: this dataset is made similarly to the first one, but only the 8 parameters of the braces are varying.

Calling p_i a generic parameter in table 3.1, we modify its reference value p_i^0 using a zero mean Gaussian distribution with standard deviation σ fixed for all the samples in the same dataset:

$$\delta = P(x) = \frac{1}{\sigma\sqrt{2\pi}} e^{-x^2/2\sigma^2} \quad (3.4)$$

The distribution of values for each parameter is centered in the reference value and its standard deviation is proportionate to it as:

$$p_i = p_i^0 (1 + \delta_i) \quad (3.5)$$

| name | reference value | description |
|-----------------------------|-----------------|---|
| Shape of the outline | | |
| r_1 | 121 mm | radius of the lower bout circle |
| r_2 | 44 mm | radius of the waist circle |
| r_3 | 88 mm | radius of the upper bout circle |
| r_4 | 43 mm | radius of the soundhole |
| $c_{1,x}$ | 55 mm | x coordinate of the center of the lower bout circle |
| $c_{3,x}$ | 45 mm | x coordinate of the center of the upper bout circle |
| $c_{1,y}$ | -108 mm | y coordinate of the center of the lower bout circle |
| $c_{2,y}$ | 52 mm | y coordinate of the center of the waist circle |
| $c_{3,y}$ | 139 mm | y coordinate of the center of the upper bout circle |
| $c_{4,y}$ | 91 mm | y coordinate of the center of the soundhole |
| w_1 | 26 mm | width of the flat part of the lower bout |
| w_2 | 26 mm | width of the flat part of the upper bout |
| Shape of the braces | | |
| s | 0.3 | scalloping factor |
| w | 7 mm | width of the cross-section |
| h_{\min} | 1.5 mm | thickness at the edges of the brace |
| h_{\max} | 3 mm | thickness at the center of the brace |
| Bracing layout | | |
| α_V | 0.6 rad | angle of the two lower braces |
| α_{fan} | 0.6 rad | angle of the fan braces |
| y_V | -161 mm | y coordinate of the center of the two lower braces |
| l_V | 130 mm | length of the two lower braces |

Table 3.1: Summary of the geometrical parameters. Graphical representation of the parameters are shown in figure 3.2 for the outline and in figures 3.4 and 3.5 for the bracing.

Since the Gaussian distribution is unbounded, to avoid distorted shapes we need to define a range of suitable values. We generate random values for δ rejecting every value until one of them lies inside the range of $\pm 2.5\sigma$. According to the probability density function, the generated values are accepted in the $\approx 98.8\%$ of the cases. Using the generation in a loop, we do not accumulate the remaining 1% of the values on the extremes of the distribution.

The standard deviation σ of the distribution of the parameters is 0.05. In the second dataset, to magnify the effect of the braces, we set $\sigma=0.2$. Considering the limitation inside $\pm 2.5\sigma$, the resulting values of δ for the first and second datasets lie in the ranges $[-0.125, 0.125]$ and $[-0.5, 0.5]$ respectively.

Using this model, we have been able to treat every parameter in the same way with the only exception of the length of the lower braces l_V . The reference value $l_V \approx 170\text{mm}$ makes the braces span almost until the outline. To keep the braces inside the soundboard, we reduce the cen-

tral value of the distribution to 130mm, affecting both the mean and the standard deviation of the values.

Instances in the dataset have also a variable number of fan braces represented by an integer random variable n_{fan} uniformly distributed between 4 and 8.

A graphical representation of the variation of the parameters is shown in figure 3.6 .

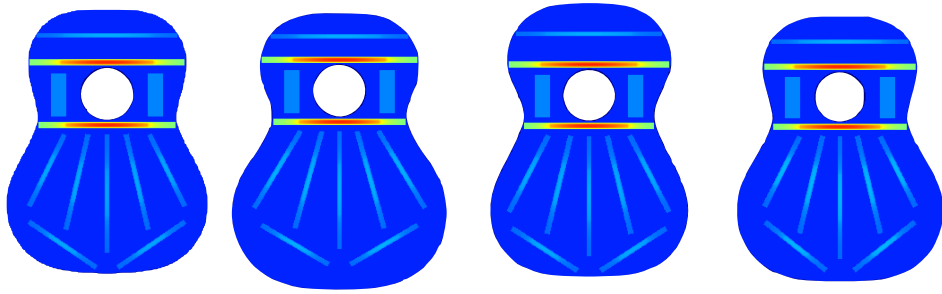


Figure 3.6: Four sample shapes from the dataset with $\sigma = 0.05$. The full set of parameters in table 3.1 is varying, the number of braces is kept constant.

3.2 Creation of the Soundboard Mesh

To create the surface of the soundboard, we evaluate in a loop each point of a gridded version of the (x, y) plane. For each point of the grid, we decide if it belongs to the soundboard and at which elevation h along the z -axis it should be placed.

The soundboard of the guitar has typically a light curvature which is modeled as a 2D Gaussian profile in the (x, y) plane as

$$h(x, y) = A \exp \left(- \left(\frac{(x - x_0)^2}{2\sigma^2} + \frac{(y - y_0)^2}{2\sigma^2} \right) \right) \quad (3.6)$$

The curve is developed in the positive direction of the z axis, with a maximum elevation of $A=3\text{mm}$. The center of the Gaussian curve is located in the bridge position (x_0, y_0) . We used the same value $\sigma=58$ to express the standard deviation in both the x and y directions.

The curvature is applied to the whole surface and to the soundhole contour, while the external outline is constrained to $z = 0$. A smoothing function is necessary to avoid abrupt changes of the slope near the edge constraint: we defined two different functions for this operation along the x and y axes respectively.

In the x-direction, we apply a sinusoidal function that gives 0 in the outline and 1 in the axis of symmetry as

$$S_x(x, y) = \sin\left(\pi/2 \frac{x - x_e(y)}{x_0 - x_e(y)}\right) \quad (3.7)$$

where we indicate with $x_e(y)$ the x-coordinate of the outline point given its y -coordinate.

To smooth out also the bottom edge y_{\min} of the soundboard, we used an arctangent function, normalized to $[0, 1]$ by the $2/\pi$ factor

$$S_y(x, y) = 2/\pi \arctan\left(10 \frac{y - y_{\min}}{y_0 - y_{\min}}\right) \quad (3.8)$$

The general expression for the elevation of a generic point of the upper surface of the soundboard is given multiplying the contributions of the curvature and the two smoothing functions as

$$z_u(x, y) = h(x, y)S_x(x, y)S_y(x, y) \quad (3.9)$$

We did not define a smoothing function in the y -direction in the top edge since the gaussian curve we defined was already flat enough in the upper bout.

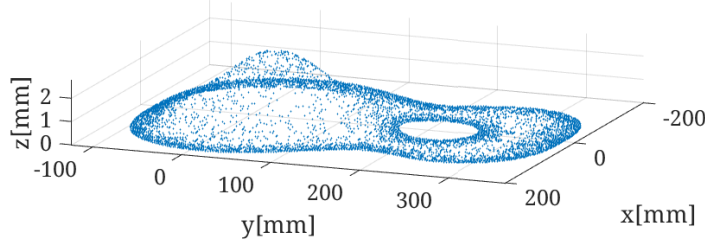


Figure 3.7: Soundboard points: z axis magnified. The (x, y) plane is centered in the center of the curve.

To lighten the resulting mesh files, we control the density of points using a random variable that prevents some points of the regular grid of the xy plane to be placed. In figure 3.7 both the lightened distribution of points and the smoothed Gaussian profile are visible. The goal is to have a large mesh size in the central part of the mesh and a finer meshing near the edges: for this purpose, we defined three coefficients measuring the distance from the outline.

$$k_x = \min\left(\frac{x - x_e(y)}{35}, 1\right) \quad (3.10)$$

The coefficient k_x accounts for the horizontal distance from the outline $x_e(y)$: it gives 0 in the outline and grows linearly up to 1 at the distance

of 35 mm.

$$k_y = \min \left(\frac{y - y_{\min}}{50}, \frac{y_{\text{top}} - y}{50}, 1 \right) \quad (3.11)$$

The coefficient k_y depends on the distance from the upper and lower bout edges y_{\min} and y_{top} respectively. Similarly to k_x it grows linearly until 1, reached at 50 mm from the extreme points in the y direction.

$$k_h = \min \left(\frac{\sqrt{(x_4 - x)^2 + (y_4 - y)^2} - r_4}{35}, 1 \right) \quad (3.12)$$

With k_h we measure the distance from the soundhole, centered in $c_4 = (x_4, y_4)$ with radius r_4 : its value grows in the 35 mm around the soundhole. The multiplication of this three coefficients gives an indication of the desired density of points in a certain position. Where the three coefficients equal one the mesh size is uniform and large, otherwise we gradually decrease it up to the edges.

The density is regulated through a comparison with a random number, generated with a uniform distribution between 0 and 1. The minimum density is realized by placing only the 15% of the points of the (x, y) grid in the mesh.

Algorithm 1 Creation of the point cloud of the soundboard starting from a grid of the (x, y) plane and applying a variable point density.

```

for points (x,y) inside outline do
  randNum ← generateRand01()
   $[k_x, k_y, k_z] \leftarrow \text{calcCoefficients}(x, y, \text{outline})$ 
  if (randNum >  $k_x \cdot k_y \cdot k_z \cdot 0.85$ ) then
    addPoint(x, y)
  end if
end for

```

Once we collected the points of the upper surface, a draft model of the mesh could be available simply replicating the points 3.5mm below along the z axis, transforming the defined surface into a solid plate. Nevertheless, to ease the union operations of all the mesh elements of the full model, the areas of contact with the braces should be properly treated. Once we created the point cloud of the braces, as described in the next section, we replicated the points of the contact face of the braces in the soundboard mesh. All the points of the soundboard which fall inside or nearby these contact areas must be removed: this operation is crucial to avoid mesh errors and intersections where the plate curvature is more prominent.

To export the meshes from Matlab[®] we created alpha shapes from the point clouds of each element. we have chosen different values for the alpha radius for each type of element we created, depending on the mesh size we used in the composition of the point cloud. For the soundboard, any value of the alpha radius that causes neither the soundhole to close nor the surface to form holes can be used. The Alpha shape object can finally be exported as an STL mesh file.

3.3 Creation of the Bracing Mesh

To create the mesh of the braces, we operated in three different ways for the transversal structural braces, the thin plates near the soundhole, and the parametric braces in the lower bout respectively. Each element in the upper bout, namely the transverse braces and the two plates next to the soundhole, is built depending only on the features of the soundboard. The braces in the lower bout are positioned and stretched depending on the parameters of the bracing layout (figure 3.5), while their thickness and width depend on specific parameters (figure 3.4).

We will define the elevation of the points of the braces as their distance dz from the soundboard. The actual coordinate of the elevation is calculated as

$$z = z_u - 3.5 - dz \quad (3.13)$$

where $z_u(x, y)$ is the elevation of the upper surface of the soundboard, calculated in equation 3.9 and 3.5 mm is the thickness of the plate.

3.3.1 Braces in the Upper Bout

The three structural braces have a fixed cross-section for all the samples, but we arranged them according to the outline and soundhole. We positioned the two thicker braces just above and below the soundhole respectively, with 4 mm of spacing from it. we have put the third brace halfway between the top point of the outline and the brace above the soundhole. All three braces fill the outline from side to side in the x-direction.

We have built the mesh of these braces one cross-section at a time along their main dimension; each cross-section is composed of three contact points with the soundboard and a curve of 11 points in the opposite edge like shown in figure 3.8.

For each cross-section we position the points p_j of the curved edge evaluating a sinusoidal function in 11 points of the arc $[0, \pi]$:

$$y_j = y_s + w_s \cos(\pi j/10) \quad \hat{z}_j = \sin(\pi j/10) \quad j \in [0, 10] \quad (3.14)$$

With w_s we indicate half the width of the transverse brace we are building, and with $\hat{z}_j \in [0, 1]$ we indicate the relative elevation of the

points inside the curve. The coordinate y_s indicates the centerline of the brace along its main direction. The actual distance dz of the points p_j from the soundboard depends on the maximum thickness of the brace h_s and the position of the cross-section along the brace.

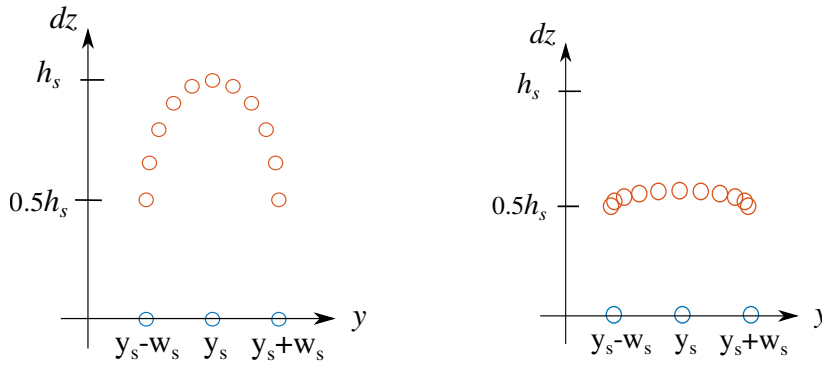


Figure 3.8: Points of the cross-sections of a brace in two different parts of the longitudinal shape. The blue points are in contact with the soundboard and the red points create the opposite face. The cross-section in the left picture is the central one ($x_n = x = 0$): it reaches the maximum thickness of the brace h_s . The cross-section in the right picture is near the edge ($x_n \approx 1$), where the curved part flattens.

To realize the curved profile of the braces along the x-direction, we evaluate the maximum elevation of each cross-section of the brace using coefficients that account for the Gaussian curvature and the scalloping. Since the three braces have different lengths, we get the scaled shapes thanks to the auxiliary term $x_n = x/x_e$, a scaled axis that represents the brace length: this axis is normalized to have $x_n = 0$ in the center of the brace and $x_n = 1$ at the edge of the braces that reach the outline in $x = x_e$ like shown in figure 3.9.

We compute the curve for $x_n \in [0, 1]$ and mirror it with respect to the y axis.

Two curves contribute to the longitudinal profile of the brace. The overall brace is characterized by a Gaussian curvature defined by

$$k_g(x_n) = \exp(-x_n^2/2\sigma^2) \quad (3.15)$$

using $\sigma = 0.6$. The scalloping curvature is represented by a piecewise-defined function

$$k_s(x_n) = \begin{cases} 1 - \sqrt{1 + \frac{x_n - 1}{x_s}} & x_s \leq x_n \leq 1 \\ 1 & 0 \leq x_n < x_s \end{cases} \quad (3.16)$$

With the value $x_s \in [0, 1]$ we indicate the normalized portion of the brace to which the scalloping is applied: we fixed it to 0.4 for all three structural braces.

Finally, the distance from the soundboard for the points of the curved face are determined multiplying the contributions of the two curvatures and the scalloping as:

$$dz_j = \frac{1}{2}h_s(1 + \hat{z}_j \cdot k_g \cdot k_s) \quad (3.17)$$

The coefficients k_g and k_s make the thickness of the curved section gradually decrease from the centre of the brace $x_n = 0$ to the edges $x_n = \pm 1$ where the thickness of the brace is half of its maximum h_s .

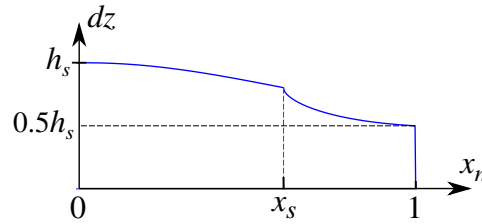


Figure 3.9: Curvature of braces along the longitudinal direction (normalized). In the interval $[0, x_s]$ the brace thickness is controlled by the gaussian curve. In the interval $[x_s, 1]$ also the scalloping is applied.

We have built one of the two flat braces next to the soundhole using 4 lines of points along the y -direction and mirrored the points with respect to the y axis to get the other plate. Their position is illustrated in figure 3.10.

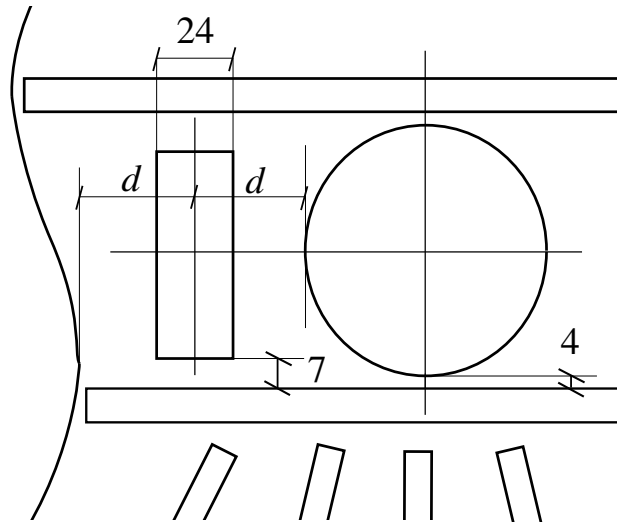


Figure 3.10: Position of the braces next to the soundhole. The dashed lines are centerlines of the brace and the soundhole. The distance d from the soundhole to the waist depends on the parameters of the outline.

The flat braces are centered between the soundhole and the waist, with a fixed width. The length of these braces depends on the size of the soundhole, which affects the position of the braces among which the plates are bounded with a fixed distance.

3.3.2 Braces in the Lower Bout

The braces in the lower bout have a shape that is very similar to the three horizontal braces in the upper bout, in fact, they all have a face characterized by a scalloped Gaussian curve, and the opposite face perfectly flattened against the soundboard. For this reason, we have built the braces in the lower bout similarly to what we have done for the structural ones with minor differences: the cross-sections are no more parallel to the y -axis, the x_n normalized axis is substituted by an axis with the same orientation of the brace; furthermore the curved part of the brace is not constrained to be half of the thickness, but two parameters independently define the thickness at the edge and at the centre.

From the main parameter set we can extract the line equation of each brace in the point-slope form $y - y_b = \tan(\theta)(x - x_b)$: this line constitutes the centerline of the brace along its main direction in the (x, y) plane, where $p_b = (x_b, y_b)$ is the center of the brace and $\theta \in [-\pi, \pi]$ defines its orientation. From the line equation, we build and align the cross-sections with central points exactly on the centerline. We add the cross-sections from the central one to the edges symmetrically, iteratively increasing of 1 mm the distance l from the central point of the bar, computing for each cross-section its center point

$$p_c = (x_b + l \cos(\theta); y_b + l \sin(\theta)) \quad l = 1, 2, \dots, L/2 \quad (3.18)$$

The other two points of the base are distanced from p_c by

$$dx = \pm \frac{w}{2} \sin(\theta); \quad dy = \mp \frac{w}{2} \cos(\theta) \quad (3.19)$$

where w is the variable parameter indicating the width of the cross-section (indicated in figure 3.4).

The curved surface of the braces is built similarly to what we did for the transverse braces in equation 3.14, but in this case the orientation is variable. Using again the coefficients dx and dy , we define the points $p_j = (x_j, y_j, \hat{z}_j)$ placed in the curved part of the cross-section as

$$\begin{aligned} x_j &= x_c + dx \cos(\pi j/10), \\ y_j &= y_c + dy \cos(\pi j/10), \\ \hat{z}_j &= \sin(\pi j/10) \end{aligned}$$

The cross-section of the braces in the lower bout can be slightly different than the structural braces ones. We have built the structural braces with a rectangular base whose thickness is half of the maximum thickness of the brace (see equation 3.17); for the braces in the lower bout instead, the two values of thickness h_{\max} and h_{\min} are independently variable giving

$$dz_j = h_{\min} + (h_{\max} - h_{\min})(\hat{z}_j \cdot k_g \cdot k_s) \quad (3.20)$$

The first braces we build are the two lower ones, for which the orientation is directly expressed by the variable parameter α_V . The centers of these two braces are distanced from the y axis by 74 mm and their y -coordinate is defined by the parameter y_V . We define the line equations of the braces by means of their central point and orientation, then we place the points of their mesh as explained in the previous paragraphs. The length of these braces is directly expressed by l_V .

The length and position of the fan braces are affected by the position of the two underlying braces: a scheme of the layout is visible in figure 3.11. To locate the fan braces we extend the line defining the lower braces to the coordinate x_{ext} that represents the extreme of the lower brace in the reference model and define the point p_{ext} there. From the point p_{ext} we draw a line with angle $\alpha_K - \alpha_V \neq \alpha_{\text{out}}$ and define the central point of the outermost fan brace p_{out} halfway between p_{ext} and the line intersection with the upper limit of the bracing y_{max} . The x coordinate of the centers of the fan braces are uniformly distributed in the range $[-x_{\text{ext}}; x_{\text{ext}}]$; similarly the angles are set to $[-\alpha_{\text{out}}, \alpha_{\text{out}}]$ with $\alpha_{\text{out}} = \alpha_K - \alpha_{\text{fan}}$. The y coordinate of these points is set to be halfway between the lower braces and y_{max} . The length of the i -th fan brace is set according to the distance of the centre from the upper limit $l_i = 2(y_{\text{max}} - y_i - 2)/\sin(\theta_i)$.

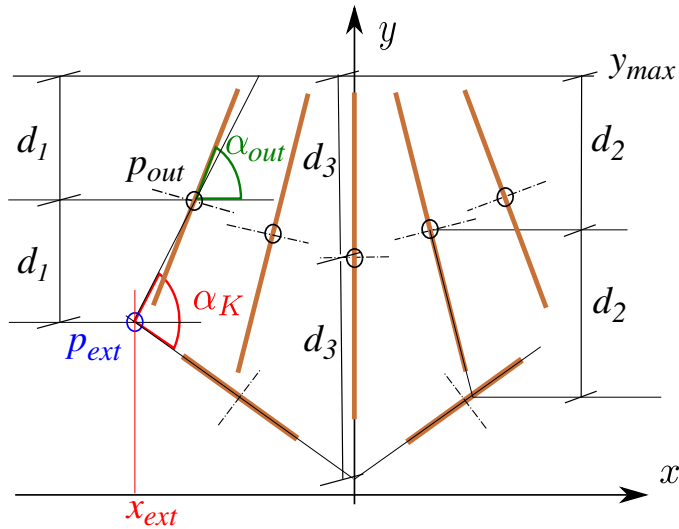


Figure 3.11: Scheme of the bracing layout assembly.

The distances d_i indicate that the centers of the fan braces, circled in black, are always placed in the middle of a line that goes from the lower braces to the upper y limit. The red values are the constants we used to locate p_{out} based on the lower braces position.

3.4 Concluding Remarks

To study the vibrating behavior of different shapes of soundboards we defined a parametric model starting from the scheme of a real guitar. From this model, we want to generate a set of different soundboards to grasp the relations between their geometrical features and their vibration modes.

We described the steps performed to get a mesh of a guitar soundboard starting from four circles. We showed our complete parametric model, built from the classical Torres guitar shape as a reference, driven by 20 geometrical parameters concerning the outline and braces. In section 3.2 we pointed out that to make the union of all the created elements work, the points of contact need to be replicated in the soundboard mesh. In the next chapter, we will go into the details of the assembly of the full mesh describing how we configured the COMSOL Multiphysics software to perform the union operation and the modal analysis.

4

Finite Element Modal Analysis of the Soundboard

In the previous chapter we presented the parametric model that allow us to generate different shapes of soundboards and bracing. The meshes generated in that way have been studied with the FEM method to analyze their normal modes.

In the first part of this chapter, we describe step by step the functionalities of COMSOL Multiphysics that we used and how we configured them to correctly assemble the meshes and analyze them. We performed the simulation of datasets of 1000 samples in a loop using MATLAB® LiveLink™, taking as input the meshes and parameters described in the previous chapter.

In the second part, we present an overview of the results of the simulations, namely the eigenfrequencies and modal shapes.

The modal shapes can undergo slight variation and their ordering on the frequency axis is often swapped, so we recognize and label them to ensure the comparison of the eigenfrequencies linked to the same shapes. The labels of the modes are assigned through a comparison with the results of the reference model that we used in the previous chapter to define the mean values of the geometrical parameters.

Finally we perform regression analysis on the first seven eigenfrequencies to obtain a prediction model.

4.1 Performing the Eigenfrequency Study in COMSOL

The soundboard meshes generated as in chapter 3 are characterized by different shapes that give them different vibrational behaviors. We are interested in analyzing the modes, characterized by different patterns of vibration called modal shapes that correspond to the natural frequencies of the structure (also called eigenfrequencies). To perform the modal analysis of the geometries, we set up a Finite Element Model simulation in the COMSOL Multiphysics software. We executed the *eigenfrequency study* of the *Structural Mechanics Module* to get the natural frequencies and vibrational modes of the soundboard assembled with the braces.

The COMSOL interface and workflow are organized in nodes and sub-nodes that are evaluated sequentially, in this section we describe our configuration node by node following the software workflow shown in figure 4.1.

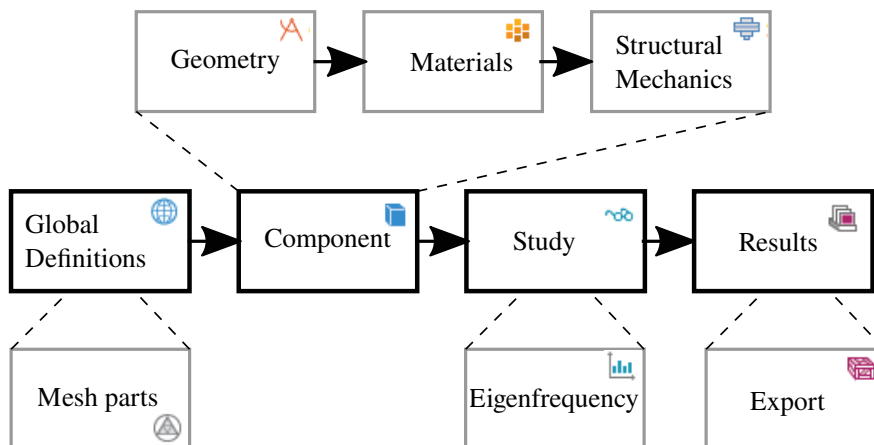


Figure 4.1: COMSOL Multiphysics workflow. The software is organized into nodes that are evaluated sequentially. Each of the 4 main nodes contains many sub-nodes, we have shown in the figure those on which we operate.

4.1.1 Mesh Parts

When importing mesh elements in COMSOL the software needs to identify edges and faces to form solid objects. The detection has to be adjusted differently for elements of different dimensions and curvature. For each sample, we import each mesh element in a different *import* node to handle the face and edge detection sensitivity independently. Each import has been defined in the *Geometry* node and generates an element under the *Mesh Parts* node.

We disabled the mesh simplifications in each import node and chose a suitable set of values for the edge and face detection fields: the sound-

board should have no edges detected in the middle of the plate, and each brace should have a plane face in contact with the plate, delimited by all its 4 edges.

If the edge detection is too strict, the bases of the braces will not be detected as planar, resulting in a rounded base not perfectly in contact with the soundboard.

If the edge detection is too sensitive, the curved parts of the braces could be spliced in smaller planar surfaces which risk causing failure when COMSOL generates their meshes.

4.1.2 Geometry

When the mesh of the soundboard and braces are imported and set up correctly, they can be joined together in the *Geometry* node using the boolean union operation. As anticipated in section 3.2, the union between the braces and the soundboard is delicate, so it is important to avoid self-intersecting curves or broken meshes otherwise the operation will not complete.

A *repair tolerance* field can be adjusted in the *Form Union* node if the operation fails: for each sample, we try different values from 0.2 and 0.6 mm until one of them works (usually the first). If all tolerances failed the simulation stops and the sample is discarded: this happened for the $\approx 3\%$ of the samples.

4.1.3 Materials

We then need to define a material for the elements: we chose the Sitka spruce, taking the mechanical parameters of the wood from [33]. An orthotropic material node has been defined for the soundboard under the *Materials* node, its elastic properties are depicted in table 4.1. Density has been set to 450 kg/m^3 .

| Young Modulus | Shear Modulus | Poisson's Ratio |
|--------------------------|----------------------|--------------------|
| $E_y = 10.8 \text{ GPa}$ | $G_{xy}/E_y = 0.064$ | $\mu_{xy} = 0.04$ |
| $E_x/E_y = 0.078$ | $G_{yz}/E_y = 0.061$ | $\mu_{yz} = 0.467$ |
| $E_z/E_y = 0.043$ | $G_{xz}/E_y = 0.003$ | $\mu_{xz} = 0.435$ |

Table 4.1: Orthotropic material model for the soundboard

We modeled the braces as made of the same wood as the soundboard, but considering their different orientations, multiple material models should have been defined to account for the different orientation of the

wood grain. To overcome the need to define a different coordinate system for each brace, we adopted a simplified solution and considered them isotropic.

We define another material with the elastic properties equal to the ones of the orthotropic one along its longitudinal direction like shown in table 4.2. The difference in the vibrating behavior between isotropic and orthotropic models for wood braces with bar shape has been measured and found negligible [34]. As Poisson's Ratio we used the coefficient μ_{tl} , relative to the deformation along the longitudinal axis caused by stress along the tangential axis [33]. Longitudinal and tangential axes are referred to the direction of the wood grains.

| Young Modulus | Density | Poisson's Ratio |
|--------------------------|----------------------|--------------------|
| $E_l = 10.8 \text{ GPa}$ | 450 kg/m^3 | $\mu_{tl} = 0.025$ |

Table 4.2: Isotropic material model for the braces

4.1.4 Solid Mechanics

In the *Solid Mechanics* node we apply the boundary conditions and the material properties to the corresponding geometric entities. We have chosen to test the soundboard in a similar configuration to its working condition, namely with the fixed boundary condition applied using the *fixed constraint* command.

To assign these conditions to the correct geometric entities, we use the *ball selection* [35] function that can be set to identify entire solids or single faces.

4.1.5 Eigenfrequency Study

In the *eigenfrequency study* node we define how many frequencies we want to find and the search criterion. We look for the first modes of the soundboard because they are the ones that most affect the tonal quality of the instrument [36]. In fact, at higher frequencies, the peaks in the frequency response are less prominent and less distanced from each other [7]. We set the solver to find the first seven frequencies around 100 Hz with a larger real part: modes with complex eigenfrequency would involve rigid motions of the structure.

4.1.6 Results

Finally, in the *results* node we export the table of the eigenfrequencies and the *solid displacement* data as CSV files. The displacement data

reports for each point of the mesh the amplitude of its vibratory motion in the z axis direction.

4.1.7 LiveLink™ scripting

To simulate a single model it is sufficient to follow the steps described above within the standard COMSOL application. Since we simulated groups of 1000 samples each, we converted the project to a MATLAB® LiveLink™ script. In this way, we automatically manage samples with different numbers of parts and apply boundary conditions and material to the actual coordinates of the elements. The coordinates of the elements are passed to the script as arguments from the function that built the meshes.

4.2 Classification of the Vibration Modes

The results of the simulation of a sample consist of seven eigenfrequencies and the related modeshapes represented by the displacement data. The modes are identified by a number from 1 to 7 corresponding to the modal shapes of the reference samples as we will explain later in the chapter. Also an indication of the nodal lines is given in the (n,m) form where n indicates the number of longitudinal nodal lines and m indicates the number of the transversal ones.

If we plot them in a histogram, the eigenfrequencies of all the modes gather in clusters resembling Gaussian curves with some overlap like shown in figure 4.2. The histogram refers to the dataset in which all the 20 parameters are varied using a Gaussian distribution with $\sigma=0.05$.

The overlaps between the frequency bands of the modes suggest that mode switching may occur. Let's take as an example the large overlap between modes 5 (0,2) and 6 (3,0), represented by green and cyan lines in figure 4.2: the fifth and sixth modal shapes of two samples can be in swapped positions if we sort them by their eigenfrequency.

We want to make sure that when we study a mode, we are actually referring to the same modal shape for all the samples, so we defined a labeling convention based on the modal shapes and not on the order of their eigenfrequencies. For this reason, we performed a simulation of the reference model characterized by the regular Torres outline and a bracing pattern involving 5 braces in a fan configuration. The modeshapes of this geometry sorted by increasing frequency are labeled with numbers from 1 to 8 and shown in table 4.3. We labeled the modes of all the samples to have them match the mode of the reference model with the corresponding label.

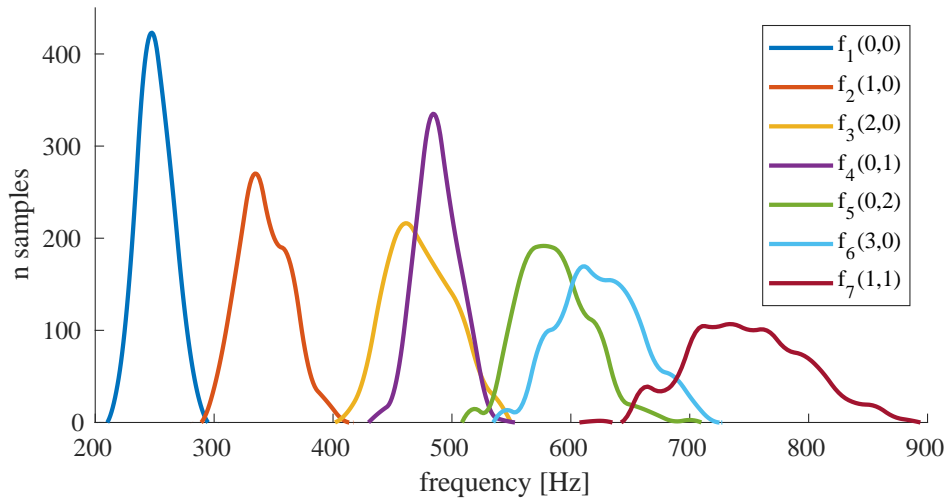


Figure 4.2: Histogram of the eigenfrequencies. Dataset of 1000 samples with all parameters variable ($\sigma = 0.05$). The different coloured distributions refer to the seven different vibration modes.

Since switching occurred between modes 7 and 8, we computed the first eight modes of the reference model to recognize both the shapes. Switching between modes 7 and 8 occurs only in forty samples, so we proceed our analysis considering only the first seven modes and neglecting the few occurrences of mode 8.

We inspected the results of the samples to find deviations with respect to the reference model. Some considerations can be also made just looking at the reference modes: for modes 3,4 and 5, the vibration area is confined neither to the upper bout nor to the lower bout, but involves both the regions to different degrees depending on the sample. In particular mode 5 is clearly a (0,2) mode in the reference model and shows an uneven vibration in the three lobes. The upper lobe vibration amplitude can be much higher with respect to the other two lobes generating a (0,0) mode in the upper bout.

In some samples, modes 3 and 4 can happen to be very similar: the most common configuration are a (2,0) mode in the lower bout and a dipole (0,1) between the upper and lower bouts with a curved nodal line like shown in table 4.3; nevertheless they tend to blend in some samples. The central lobe of mode 3 can extend to different degrees in the upper bout, while mode 4 can see its nodal line so curved that it makes the lower bout resemble a (2,0) mode; this tendency to blend and the little difference of the eigenfrequencies make these modes quite difficult to distinguish, as visible in figure 4.3.

We automatically recognize the mode shapes from the displacement data exported by the simulations. To do so, we define a 2D representation

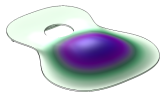
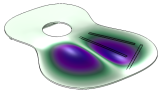
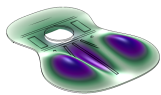
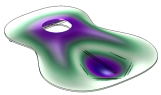
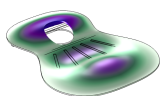
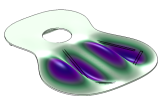
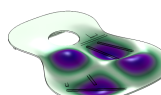
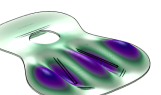
| shape | label | shape | label |
|---|----------------------------------|--|----------------------------------|
|  | Mode 1 (0,0) 251 Hz |  | Mode 2 (1,0) 342 Hz |
|  | Mode 3 (2,0) 474 Hz |  | Mode 4 (0,1) 495 Hz |
|  | Mode 5 (0,2) 580 Hz |  | Mode 6 (3,0) 632 Hz |
|  | Mode 7 (1,1) 746 Hz |  | Mode 8 (4,0) 814 Hz |

Table 4.3: Modal shapes of the reference model. This model is not taken from the dataset, it is equivalent to a sample in which all the parameters are set to the mean value of their distributions.

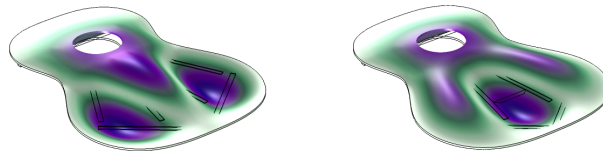


Figure 4.3: From left to right, modes 3 and 4 variants, belonging to the same sample

of the guitar plate employing a grid of the (x, y) plane limited inside the outline of the sample. The vibration amplitude given as scattered data for the mesh of points created by COMSOL, is fitted to the grid using the `griddata` function of MATLAB®. This function builds a Delaunay triangulation of the scattered data and evaluates the vibration amplitude in the grid points through linear interpolation [37].

To classify the modal shapes of samples characterized by different geometries we need to recognize the vibration patterns from the gridded displacement data. For this reason, we used the two-dimensional Fourier transform, which detects the harmonic components of the input data along its two dimensions. We performed the 2D Fast Fourier Transform

algorithm on the gridded data of each modeshape of each sample, including the reference one. Since the spatial sampling resolution we used is high relative to the size of the vibration lobes, we evaluate the 10 bins closest to the zero spatial frequency in the two dimensions. Each shape is thus represented by a 10x10 matrix in the spatial frequency domain. Two examples of these matrix are shown in figure 4.4.

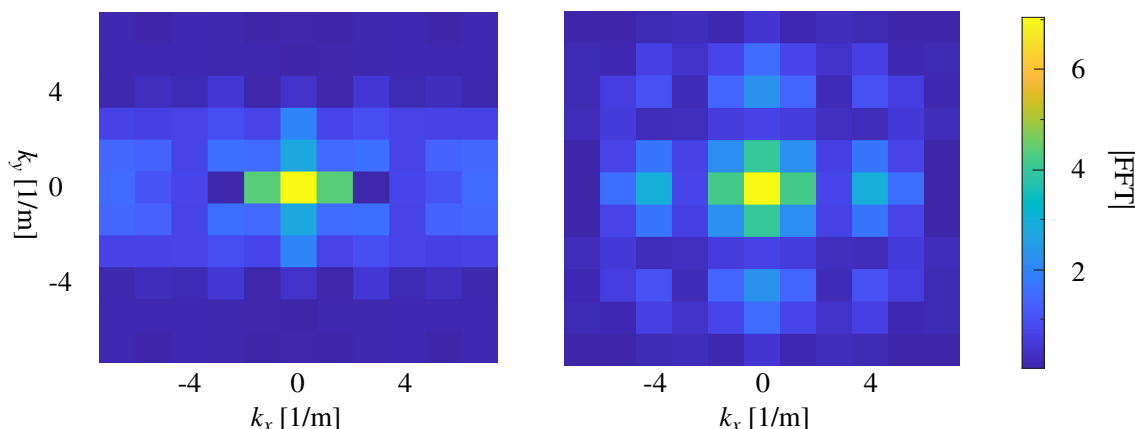


Figure 4.4: Fourier transform of the displacement data of modes 3 (0,2) and 7 (1,1). k_x and k_y represent the wave number of the spatial frequency bin in the two directions x and y .

Then, for each mode of the samples, a comparison with each one of the 8 modeshapes of the reference model is performed through a simple element-wise subtraction of the 10x10 matrix as shown in equation 4.1.

$$\Delta_{\text{FFT}}(j) = \sum_{h=1}^{10} \sum_{k=1}^{10} |\text{FFT}_s(i, h, k) - \text{FFT}_{\text{ref}}(j, h, k)| \quad (4.1)$$

$\text{FFT}_s(i, \cdot, \cdot)$ and $\text{FFT}_{\text{ref}}(j, \cdot, \cdot)$ are the 10x10 matrices of modes i and j of the sample and the reference model respectively.

For each computed mode, the assigned label is the one for which the difference between the reference modeshapes and the shape under analysis is the minimum.

$$\text{Label}(i) = \min_j \Delta_{\text{FFT}}(j) \quad (4.2)$$

After all the modeshapes have been compared, for each sample we check that there are not two or more modes marked with the same number. Otherwise, a final check is made on the labels since wrong identification with this method can happen, especially for modes 4 and 6.

Mode 4 (0,1) can be identified as 1 (0,0) or 3 (2,0) due to its strongly variable shape; so when one of these two labels is duplicated the one with higher frequency is usually the correct mode 4.

Mode 6 (3,0) can be identified as 3 (2,0) or 8 (4,0) because they all develop nodal lines which are parallel to the y axis, but also in this case the correction is pretty straightforward. It is sufficient to notice the presence of three modes of this kind and make sure that the three occurrences are marked respectively as 3, 6 and 8 if sorted by increasing frequency.

The correction of duplicates is based on the observation of the labels assigned to the data, so it has to be adjusted with respect to the dataset. The errors that are fixed in this way are systematic and involve a minor part of the samples ($\approx 5\%$) so we supervised this phase to get the correct labels where the automatic labeling failed.

The complete procedure of mode labeling for a full dataset is synthesized in the algorithm 2.

Algorithm 2 Automatic mode labeling.

```

FFTref ← Calculate FFTs of reference modes           ▷ 9 matrices
for samples S do
  FFTs ← Calculate FFTs for the sample S           ▷ 7 matrices
  for  $i_s = 1, 2 \dots 7$  do                         ▷ Loop sample modes
    for  $j = 1, 2 \dots 9$  do                       ▷ Loop reference modes
       $\Delta_{\text{FFT}}(j) \leftarrow$  Compute difference (equation 4.1)
    end for
    Label( $i_s$ ) ← Index with minimum difference (equation 4.2)
  end for
  Resolve duplicate labels
end for

```

4.3 Eigenfrequencies Prediction from Geometrical Features

Since we recognized and classified the modes as described in the previous section, we now refer to a generic mode n with eigenfrequency f_n as the n -th mode of table 4.3. The 40 samples that have the mode 7 switched with mode 8, do not contribute to the prediction model for mode 7 because it is missing from its first 7 modes.

Our dataset includes $N=1000$ samples, each one described by a set of 20 geometrical parameters as possible predictors and seven eigenfrequencies as outcomes.

To understand the influence of the geometrical parameters of the soundboard with bracing on the frequency of its normal modes we look for a function that relates them

$$\mathbf{f} = f(\mathbf{x}) \tag{4.3}$$

where \mathbf{x} is the vector of the parameters and \mathbf{f} is the vector of the seven eigenfrequencies.

We have chosen to perform polynomial regression, looking for models that best describe these relations in the form:

$$\hat{\mathbf{f}} = \mathbf{b}_0 + \mathcal{B}_1 \mathbf{x} + \mathcal{B}_2 \mathbf{x}^2 + \boldsymbol{\epsilon} \quad (4.4)$$

where \mathbf{b}_0 is a constant term, $\mathcal{B}_1, \mathcal{B}_2$ are matrices of the coefficients of the 20 parameters contained in vector \mathbf{x} , and $\boldsymbol{\epsilon}$ represents the prediction error. The vector $\hat{\mathbf{f}}$ represents the predicted eigenfrequencies for the first seven modes, classified with the method described in the previous section. Since the relation between the coefficients and the dependent variable is linear, our model is equivalent to a multiple linear regression that treats \mathbf{x} and \mathbf{x}^2 as two independent variables. The coefficients $\mathbf{b}_0, \mathcal{B}_1, \mathcal{B}_2$ are calculated through the least-squares method, and the reliability of the fitted model is measured with the coefficient of determination

$$R^2 = 1 - \frac{\sum_{i=1}^N (f_i - \hat{f}_i)^2}{\sum_{i=1}^N (f_i - \bar{f})^2} \quad (4.5)$$

where f_i and \bar{f} are the actual values and mean value of the eigenfrequencies calculated with the simulations and \hat{f}_i are the values calculated through the model.

We performed regression analysis using the `polyfitn` function in Matlab [38] that allows the polynomial fitting of multiple independent variables simultaneously. The coefficients of determination in table 4.4 give an indication of the accuracy of the fitting.

| | f_1 | f_2 | f_3 | f_4 | f_5 | f_6 | f_7 |
|-------|-------|-------|-------|-------|-------|-------|-------|
| R^2 | 0.989 | 0.983 | 0.977 | 0.912 | 0.950 | 0.944 | 0.962 |

Table 4.4: Regression performance: R^2 values of quadratic regression for the 7 modes. All parameters varying ($\sigma=0.05$).

When evaluating the performance of the regression model we have to keep in mind that the variation of the number of braces is not included in the predictor set, so it can increase the prediction error and affect the regression performance.

The contribution of each parameter in the model is different: some of them happen to be almost irrelevant for the eigenfrequency prediction, while a few others are sufficient to reach considerable accuracy. Figure 4.5 shows the fastest way to reach the maximum performance of linear regression iteratively adding one parameter at a time.

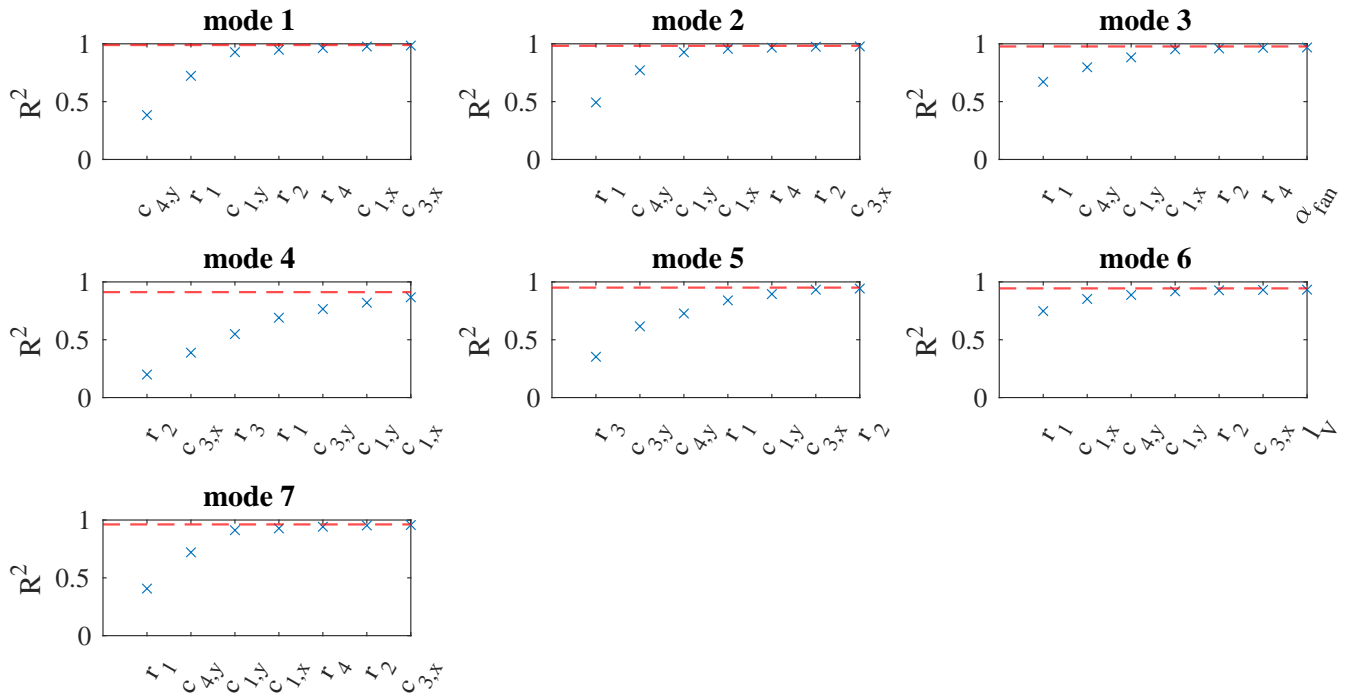


Figure 4.5: Performance of the quadratic regression incrementing the number of parameters from 1 to 7. Each increment involves the parameter that maximizes the R^2 index. The red line represents the maximum R^2 corresponding to the regression of all the 20 parameters listed in table 3.1

For each mode, seven parameters or even fewer ones are sufficient to achieve a R^2 value that is very near to the maximum one represented by the red line. The model seems to be very simple especially for the prediction of modes that vibrate in the lower bout: four parameters concerning the lower bout and the soundhole are sufficient to have a good prediction of frequencies 1, 2, 3, 6, and 7. This shows that some parameters are much more influential than others in the prediction model, mainly because the effect of some geometrical features on the frequencies may vary considerably between different parameters.

We recall that the parameters of the outline are visible in figure 3.2 and the whole parameter set is described in table 3.1.

To get a complete overview of the relations between eigenfrequencies and parameters we calculate also the correlation matrix of the dataset: the submatrix relating geometrical parameters to the eigenfrequencies is visible in figure 4.6. Even if the correlation coefficient r does not imply an actual dependence this picture well represents our data, in fact, the highest-scoring values in this matrix correspond to the most influential parameters shown in figure 4.5. We got a nearly identical picture also representing the linear terms of regression, weighted by the reference

value of the corresponding parameter, in a matrix form: the parameters highlighted for the greater contribution are the same. The actual values of the regression coefficients are shown in tables in appendix A.

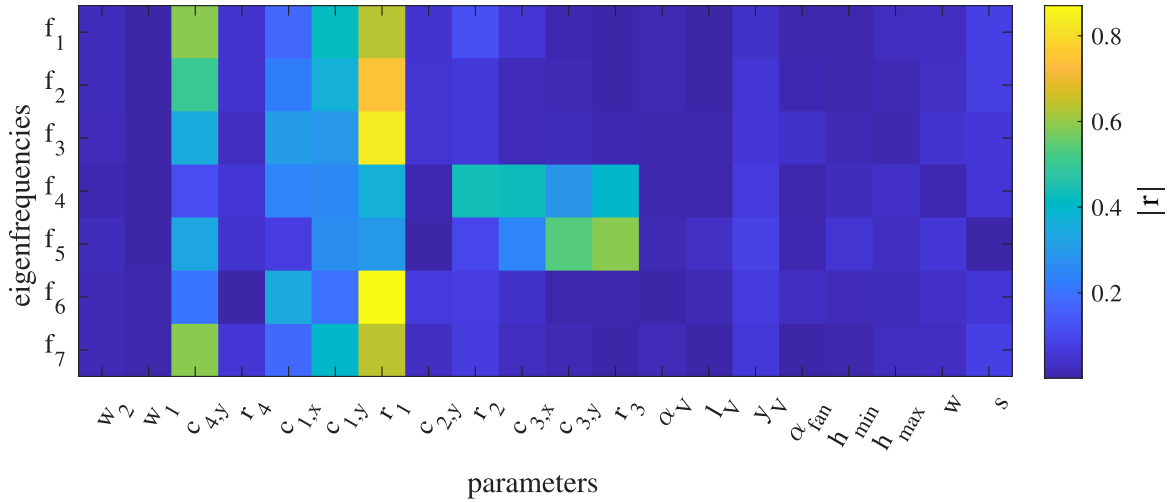


Figure 4.6: Correlation coefficients of the 20 geometrical parameters listed in table 3.1 with the 7 eigenfrequencies. All parameters are varying with $\sigma = 0.05$ and described in table 3.1.

What is most evident across the whole parameter set is the dominance of the two bouts and the soundhole over all the other parameters in the dataset. In particular, the longitudinal position of the soundhole $c_{4,y}$ and the radius of the lower bout indicated by r_1 , are strongly correlated with the frequencies of the modes that resonate in the lower bout.

Modes 4 and 5 are the only ones that involve a relevant vibration of both the upper and lower bouts as suggested by the reference modal shapes in table 4.3. This is coherent with the lower correlation with r_1 and the higher correlation with the upper bout circle c_3 compared to all the other modes.

The common thread between these results is the limitation of the vibrating area as the main contribution of the geometrical features to the regression model and to the frequencies.

On the other hand, parameters that do not affect the size of the vibrating surfaces have minimum relations with the eigenfrequencies. For example, the width of the flattened edges of the outline is negligible both in terms of correlation and in terms of contribution to the regression model. The same holds for the longitudinal position of the waist.

These three parameters in fact change more the shape of the guitar rather than the actual dimensions of the vibrating areas.

The transversal brace just below the soundhole has a role of structural support but also delimits the vibrating area of the lower bout [7], so its position can affect the modes that vibrate in that area. In our model, the soundhole position affects the eigenfrequencies indirectly because it determines the position of this brace. Examining the correlations with the frequencies, we found nearly identical values for the positions of the soundhole and the underlying brace.

The soundhole radius instead has minor effects because its mean value is way less than the value of its position: hence its effect on the position of the underlying brace is less.

One possible implication is that for the considered bracing system the size and position of the soundhole can be independently chosen to control the resonances of the air cavity and the plate, respectively. In fact, the guitar body also acts as a Helmholtz resonator, which resonant frequency is determined by the volume of the body and the radius of the hole [7]. In the case of different bracing systems that ease the propagation of the vibrations outside the lower bout instead, the implications about the soundhole position would not hold.

The fourth mode (0,1) is the most complex to predict, in fact, no particularly relevant parameter that influences the behavior of this mode is visible both in figure 4.5 and 4.6. This is the mode that is most affected by the waist r_2 with a correlation of only 0.44, but there is not a single parameter that noticeably affects its frequency more than others.

We tried to combine different parameters to see if some features score higher correlations with this mode. We found the highest correlation with the mean width of the outline scoring 0.67, but this actually correlates in a similar measure to all the 7 eigenfrequencies.

The mode that is most involved with the upper bout is the fifth one (0,2) because among its three lobes the one that vibrates there is the most prominent. The fifth eigenfrequency has the strongest relations with the parameters of the upper bout but the correlation values are not as high as the ones regarding the lower bout modes. Summing the contribution of $c_{3,y}$ and r_3 we obtain the y coordinate of the neck joint for which the correlation with the fifth frequency increases to 0.75. This noticeable increment suggests again that the size of the vibrating area has a more direct effect compared to the form factor.

Correlation helps us interpret the moderate contribution of the waist and upper bout parameters, but can not help highlighting the minimal role of the bracing parameters.

Neither regression coefficients nor the correlation ones show relevant contributions of the braces in the lower bout. For this reason, we decided to dedicate a study case on them and understand the degree to which they influence the soundboard modes.

4.4 Bracing Influence on Eigenfrequencies

The dataset used for the study of the fan bracing is characterized by the variation of the 8 parameters concerning the bracing layout and the shape of the struts, while the other 12 parameters concerning the outline are fixed to the values of the reference model.

We recall that in table 3.1 the parameters of the bracing are described and separated by the ones of the outline, while figures 3.4 and 3.5 represent their geometrical interpretation.

The distribution of the parameters values in this dataset is characterized by a standard deviation $\sigma=0.2$ which is four times larger than the one used in the previous study case.

The resulting samples are characterized by a standard Torres outline and a fan bracing pattern that varies significantly more than the one in the dataset analyzed before. The number of braces is uniformly distributed from 4 to 8 elements in fan configuration exactly like in the previous dataset.

It turns out that the variation of the frequencies is very low compared to the previous case, the difference is immediately visible in the histogram shown in figure 4.7.

The distribution still includes overlaps, but it is much narrower than the one shown in figure 4.2.

To compare the variations in the two datasets, we report the standard deviations in table 4.5, expressed as percentages with respect to the mean values of the frequencies.

| | f_1 | f_2 | f_3 | f_4 | f_5 | f_6 | f_7 | μ_f |
|------------------------|--------|--------|--------|--------|--------|--------|--------|---------|
| $\sigma_{20}[\%]$ | 6.0849 | 6.3319 | 5.8724 | 3.7625 | 5.1808 | 5.6335 | 6.5007 | 5.6238 |
| $\sigma_8[\%]$ | 1.2551 | 1.6113 | 1.8647 | 0.7469 | 1.0412 | 2.6230 | 1.9130 | 1.5793 |
| σ_{20}/σ_8 | 4.8483 | 3.9298 | 3.1492 | 5.0374 | 4.9757 | 2.1478 | 3.3982 | 3.5610 |

Table 4.5: Standard deviation of the frequencies calculated with the numerical simulations, compared between the two datasets. Pedices indicate the number of varying parameters: σ_{20} refers to the completely variable dataset and σ_8 refers to the bracing varying one. The mean of the seven values of the standard deviation is expressed as μ_f .

On average, the frequency variation of the second dataset is 3.5 times lower than the first one despite the geometrical parameters have a four times higher variation. Hence the thin braces show only a small influence for what concerns the eigenfrequencies.

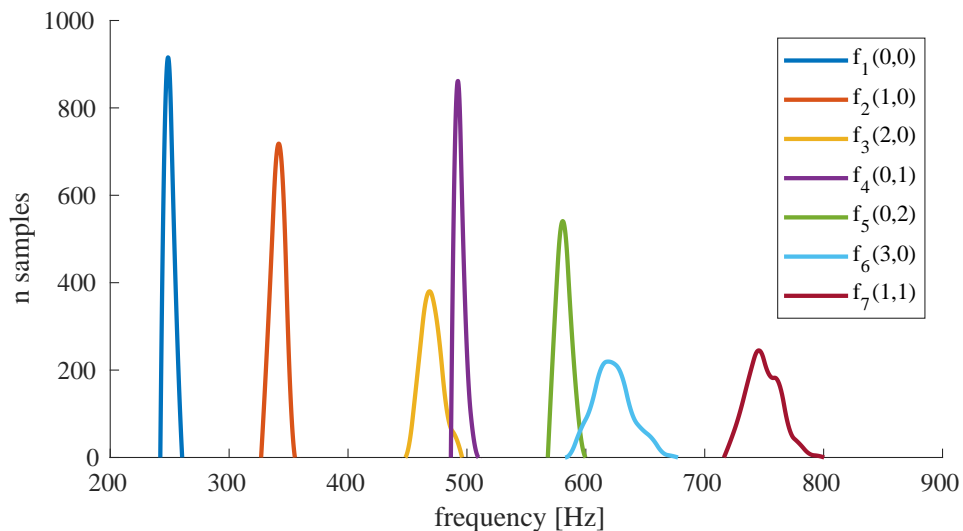


Figure 4.7: Histogram of the eigenfrequencies. Dataset of 1000 samples with only bracing parameters variable ($\sigma=0.2$).

This is coherent with the tradition of guitar making, as different families of guitars employ different soundboard shapes to adapt to different ranges or features of the instrument [16]. Steel string guitars or baritone guitars for instance have different outlines than classical guitars. On the other hand, fine-tuning of the plate can be performed when the main guitar characteristics are defined. To do so, braces are carved when already assembled with the soundboard

Since the bracing system we are studying is entirely confined to the lower bout, the modes that have both vibration lobes and nodal lines in that area are the most affected. Indeed, modes 3, 6 and 7, are the ones that have a variation significantly above the average.

On this dataset we performed the same kind of regression as shown in the previous section. The performance in this case is decreased as visible in table 4.6.

| | f_1 | f_2 | f_3 | f_4 | f_5 | f_6 | f_7 |
|-------|-------|-------|-------|-------|-------|-------|-------|
| R^2 | 0.841 | 0.798 | 0.871 | 0.759 | 0.571 | 0.691 | 0.607 |

Table 4.6: Regression performances: R^2 values of quadratic regression for the 7 modes. Eight parameters varying ($\sigma=0.2$)

The lower performance of the linear regression model led us to try alternative methods for the prediction of the eigenfrequencies. Inspired by the excellent results obtained on violins [34], we tried to use a feedforward neural network to improve the accuracy of the model. The network does not perform consistently better, even trying different

numbers of neurons and layers, so we adopted also for this analysis the quadratic regression as our prediction model.

The contribute of each parameter to the regression model is shown in figure 4.8.

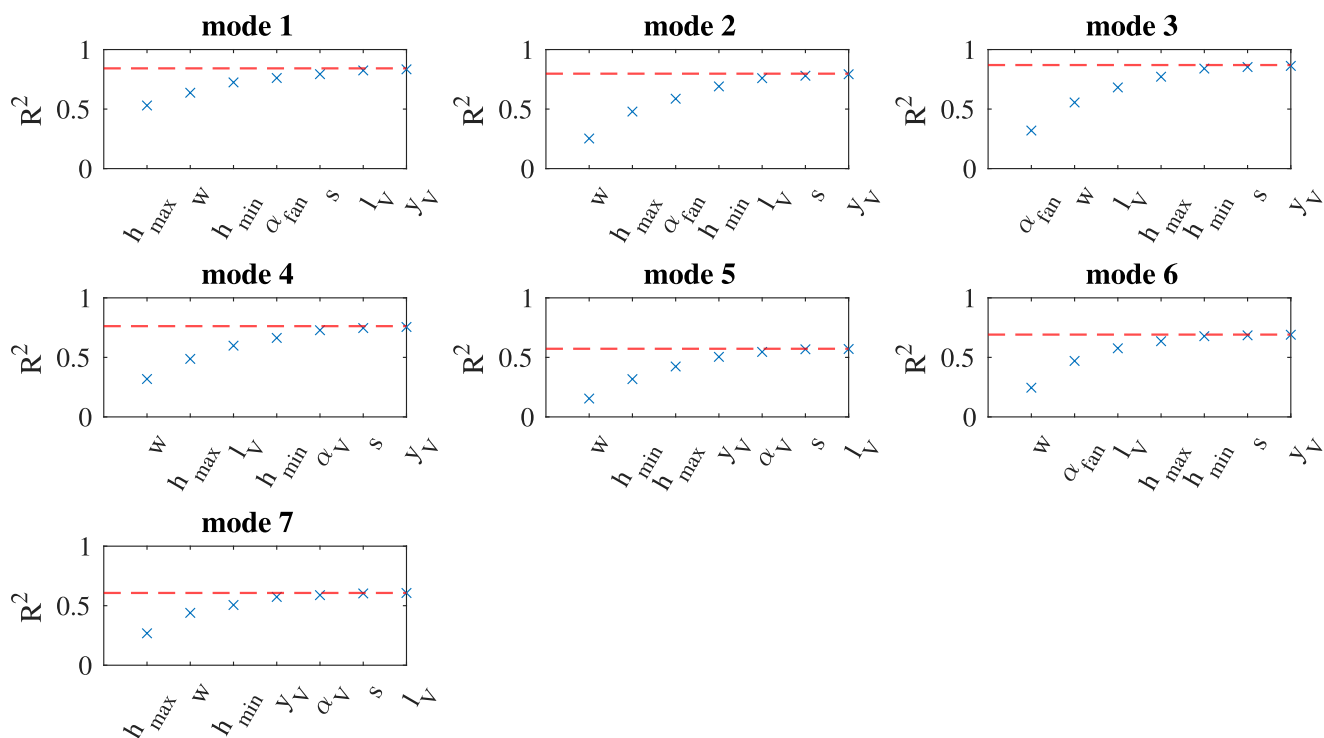


Figure 4.8: Performance of the quadratic regression, incrementing the number of parameters from 1 to 7. Each increment involves the parameter that maximizes the R^2 index. The red line represents the maximum R^2 achieved with all the 8 parameters.

The size of the cross section of the braces is a main contribution across all the modes, as indicated by the parameters h_{min} , h_{max} , w . These three parameters show a positive correlation with the frequency, meaning that larger cross sections happen to make the lower bout stiffer.

The angles of the braces α_{fan} , α_V affect mainly modes 2, 3 and 6, in which the nodal lines develop in the longitudinal direction of the soundboard. The only case in which one parameter is enough to reach half of the maximum R^2 is the contribution of h_{max} in the first mode.

The correlation of the brace thickness is linked to the role of the cross-section shape in stiffening a bar: a tall brace has a grater stiffening contribution to bending than a large flat one [7]; this is highlighted for the first mode because no brace lies on a nodal line so all braces contribute in stiffening the plate against the vibration.

The different contribution of mass and stiffness of the fan bracing has been addressed also in [10] where the addition of more braces raised the

lower frequencies of the soundboard and lowered the higher ones: this suggests that at lower frequencies the braces contribute more in terms of stiffness, while at higher frequency they act as weights.

The contribution of the regression terms are very low with respect to the previous case as the narrower distribution suggests. The magnitude of the regression terms follows the width of the frequency distributions, having minimum coefficients for mode 4 and larger ones for modes 3 and 6.

The parameters that most contribute to the regression like shown in figure 4.8 are the ones that have the higher regression coefficients. This indicates that despite the small variation of the outcomes and the lower scoring R^2 , the model is still considerably accurate.

The complete table of the calculated regression coefficients is visible in appendix A.

We performed the same kind of regression analysis on the subset of data that have 5 fan braces. The results are once again coherent with what shown in this section, reporting the size of the cross sections of the braces as main contributions for almost all the modes and the angle α_{fan} as relevant for modes 3 and 6.

In a complementary way, we looked at the role of the number of braces and compared it to the brace size. As visible in figure 4.9, the total volume of braces V is more correlated with the frequencies than the single dimensions as it sums up their contributions.

it is interesting to notice that the first modes seem more affected by the size of the braces expressed by the ratio V/n , while modes 5 and 7 have higher correlation with the number of braces n instead. This can be partly explained by the role of the brace position with respect to the vibration lobes. While mode 1 senses a diffused stiffening of the surface, higher modes with their small vibration lobes are differently affected if the braces are positioned near the nodal lines or near the peak of the vibration lobes.

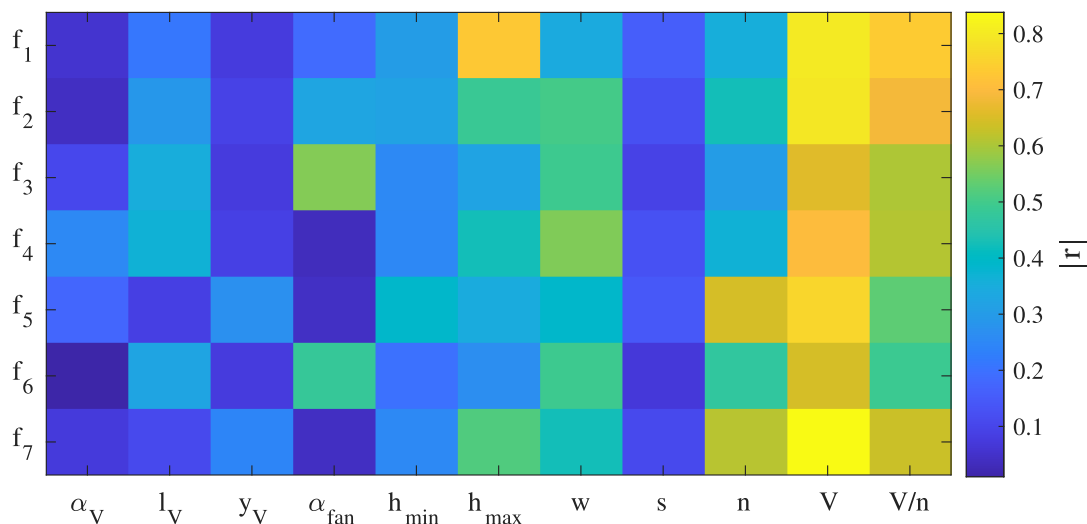


Figure 4.9: Correlation coefficients in the varying bracing case. The last three variables on the x axis are the total bracing volume V , the number of braces n and the ratio between the two. These parameters are derived from the other 8 ones, which are described in table 3.1 in the rows related to the bracing.

4.5 Concluding Remarks

In this chapter, we have shown how we performed the modal analysis of datasets of guitar soundboards and inferred some relations between their geometry and vibrational behavior.

The parametric model described in chapter 3 has been used to generate the mesh of all the samples we analyzed, and its parameters have been used as predictors of the eigenfrequencies in a regression model. We made separate datasets for the full variation of the model and the only variation of the lower bout bracing. The full model analysis gives a broad picture of the main contributions that sensibly raise or lower the resonant frequencies of the plate and the whole instrument.

Since the contributions of the braces are way less effective than the outline features, we performed a dedicated study on it and found how the different eigenfrequencies are affected.

The regression coefficients for both the studies are reported in the appendix A. With these coefficients, one can calculate the eigenfrequencies of a custom plate from its geometrical features with neither a FEM simulation nor a concrete realization of it. This can be an additional tool in the design process both for the luthier workshop and the industry.

5

Conclusions and Future Works

This work of thesis presents a methodology to draw the relations between geometrical features of the classical guitar soundboard and the resulting vibratory response. The results of this work can be used in the design phase to adjust the construction features in order to achieve a certain tone on the finished instrument.

We focused our study on the shape of the Torres guitar top plate and the features of the fan bracing.

Using a parametric model, we generated different braced soundboard samples on which we performed Finite Element Modal Analysis. Numerical simulations allow us to inspect the vibrational behavior of many soundboards without actually building or borrowing them.

The regression analysis we performed on the construction parameters provides a simple model to predict the eigenfrequencies we calculated with the numerical simulations. The linear equation built with the regression coefficients can be used also as an approximation for geometries not included in our dataset but with a reasonable similarity.

The proposed approach has shown good reliability. The statistical analysis reported relevant correlations and good performance, giving results that are coherent with the literature.

We show that the relations between the geometrical parameters and the vibration modes of the soundboard are well described by quadratic functions and we provide the formula and coefficients needed to predict the first seven eigenfrequencies of any soundboard shape with fan bracing that complies with our model. This formulation constitute an important progress with respect to the empirical methods employed by luthiers and

it is way faster than performing a numerical simulation.

5.1 Future Works

Despite the analysis of 20 different parameters and the variation of the number of braces in the fan layout, our study is still focused on a very specific type of guitar soundboard and bracing.

Other parameters and constructive aspect need to be studied to make this model more general: parametric material properties, a variable thickness profile along the soundboard, parametric arching of the plate and asymmetric shapes can be used for example.

Including other parameters would make the model more complex; as a consequence, different regression models like neural networks should be tested to check for relevant improvement in the prediction.

Apart from adding parameters to this model, two different approaches can be adopted to further extend this research. The first one consists of adding more elements to the simulations, starting from the bridge plate that acts as an additional brace. The addition of elements can be extended to different degrees until the whole guitar is included.

The second approach is to build other parametric models to account for all the guitars we do not consider in our study. The comparison of different guitar types and bracing systems cannot be represented by continuously distributed parameters like the ones we used but would constitute new study cases for which our methodology would be interesting to apply.

For what concerns the bracing, there is a huge variety of configurations used by luthiers that would be inefficient to cover with as many study cases. For this reason, developing a model in which the braces are randomly distributed in the soundboard would be an interesting approach to generalize their effect on the soundboard vibration, opening the possibility of a parametric design of new bracing systems.

Finally, the use of metamaterials for the construction of soundboards is becoming widespread thanks to claims about its good tonal quality and its louder radiation [7]. Studies on soundboards made of these materials should be performed to validate and measure the difference with plain wood ones.

Metamaterials have singular mechanical properties [39] that turned useful in many applications. Acoustic applications are mainly studied to control noise, employing analysis methods similar to the ones we showed for soundboards [40].

Therefore, the modal analysis with parametric shapes we performed on classical guitar and already studied on violins in [34] could include different materials and find a wide field of application also outside musical acoustics.

My Appendices

A Tables of the Regression Coefficients

The tables shown in this section refer to the regression study described in section 4.3. The rows correspond to the 20 geometrical parameters described in table 3.1 and illustrated in figures 3.2 and 3.5. The seven eigenfrequencies f_i correspond to the first seven modal shapes shown in table 4.3.

| | f_1 | f_2 | f_3 | f_4 | f_5 | f_6 | f_7 |
|----------------|----------|----------|----------|----------|---------|----------|----------|
| w_2 | 1.1 | -4.7 | 0.17 | 17 | -0.31 | -8.7 | 10 |
| w_1 | 2 | 3.2 | -2 | 9 | 7.3 | 7.2 | 8.7 |
| $c_{4,y}$ | -1.9 | -4.9 | -4.7 | 6.2 | -7.3 | -3.9 | -10 |
| r_4 | 2.2 | 2.6 | 2.4 | -2 | 4.3 | 1.6 | 10 |
| $c_{1,x}$ | 1.7 | 3.7 | 6 | 0.85 | 6.4 | 10 | 8.3 |
| $c_{1,y}$ | -2 | -4.2 | -4.3 | 0.41 | -3.3 | -4.7 | -8.1 |
| r_1 | -2.5 | -6.1 | -11 | 4.7 | -4.2 | -13 | -11 |
| $c_{2,y}$ | 0.82 | 0.79 | -0.14 | 0.55 | -1.9 | -1.6 | 1.3 |
| r_2 | 3.4 | 2.5 | 2 | 10 | -5 | 12 | 17 |
| $c_{3,x}$ | 1.2 | 1.9 | 4.9 | -0.25 | 5.9 | 4 | 2.5 |
| $c_{3,y}$ | -0.25 | -0.54 | -1.9 | 3 | -13 | -1.3 | -1.7 |
| r_3 | 0.11 | 0.2 | -1.1 | 8.4 | -16 | 2.9 | 0.95 |
| α_V | 70 | 75 | 2.2e+02 | -76 | 2.6e+02 | 1.5e+02 | 2.7e+02 |
| l_V | -0.11 | -0.12 | -0.43 | 0.27 | 0.15 | 0.15 | -0.44 |
| y_V | -0.45 | -0.27 | -2.4 | 2.3 | -1 | -0.84 | -0.15 |
| α_{fan} | 23 | -3.6 | -33 | -38 | 2.3e+02 | 1.8e+02 | -45 |
| h_{min} | -10 | -12 | 30 | -99 | 94 | 37 | -1.8 |
| h_{max} | -29 | -52 | -64 | 44 | -79 | -1.2e+02 | -1.6e+02 |
| w | 4.7 | 5 | -18 | 18 | -17 | -22 | -3.5 |
| s | -1.4e+02 | -2.6e+02 | -2.6e+02 | -8.6e+02 | 1.2e+02 | -1.1e+03 | -1.3e+03 |

Table 1: Linear terms \mathcal{B}_1 of regression coefficients, dataset of 20 varying parameters ($\sigma = 0.05$)

| | f_1 | f_2 | f_3 | f_4 | f_5 | f_6 | f_7 |
|----------------|---------|---------|----------|---------|----------|----------|---------|
| w_2 | -0.047 | 0.18 | -0.0063 | -0.66 | -0.00082 | 0.34 | -0.39 |
| w_1 | -0.077 | -0.12 | 0.083 | -0.35 | -0.27 | -0.26 | -0.32 |
| $c_{4,y}$ | 0.0021 | 0.0088 | 0.0086 | -0.015 | 0.019 | 0.0076 | 0.017 |
| r_4 | -0.016 | -0.017 | -0.017 | 0.032 | -0.043 | -0.014 | -0.088 |
| $c_{1,x}$ | 0.0097 | 0.021 | 0.029 | -0.006 | 0.052 | 0.053 | 0.055 |
| $c_{1,y}$ | 0.0033 | 0.012 | 0.013 | -0.0056 | 0.0089 | 0.016 | 0.018 |
| r_1 | 0.004 | 0.014 | 0.031 | -0.024 | 0.01 | 0.031 | 0.025 |
| $c_{2,y}$ | 0.0061 | 0.0051 | -0.005 | 0.0073 | -0.016 | -0.022 | 0.0094 |
| r_2 | -0.027 | -0.018 | -0.0094 | -0.07 | 0.072 | -0.12 | -0.16 |
| $c_{3,x}$ | 0.0057 | 0.015 | 0.048 | -0.043 | 0.034 | 0.034 | 0.011 |
| $c_{3,y}$ | 0.00079 | 0.0019 | 0.0069 | -0.014 | 0.039 | 0.0045 | 0.0059 |
| r_3 | -0.0008 | -0.0014 | 0.0065 | -0.057 | 0.069 | -0.017 | -0.0059 |
| α_V | -53 | -56 | -1.9e+02 | 79 | -2.1e+02 | -1.2e+02 | -2e+02 |
| l_V | 0.00052 | 0.0007 | 0.0023 | -0.0008 | -0.00057 | 0.00039 | 0.0019 |
| y_V | -0.0042 | -0.0017 | -0.024 | 0.025 | -0.0075 | -0.0076 | 0.0053 |
| α_{fan} | -12 | 22 | 78 | 23 | -1.9e+02 | -81 | 48 |
| h_{min} | 4.1 | 5.8 | -6.9 | 33 | -28 | -9.6 | 3.2 |
| h_{max} | 5.7 | 9.6 | 12 | -6.7 | 14 | 22 | 30 |
| w | -0.32 | -0.28 | 1.6 | -1.3 | 1.2 | 1.8 | 0.35 |
| s | 2e+02 | 4e+02 | 4.1e+02 | 1.4e+03 | -2.2e+02 | 1.8e+03 | 2.1e+03 |

Table 2: Quadratic terms \mathcal{B}_2 of regression coefficients, dataset of 20 varying parameters ($\sigma = 0.05$)

| | f_1 | f_2 | f_3 | f_4 | f_5 | f_6 | f_7 |
|-----------------------|-------|-------|---------|--------|--------|-------|-------|
| α_V | -0.54 | -5.7 | 3.1 | 2.6 | -4.3 | -32 | -63 |
| l_V | 0.017 | 0.089 | 0.19 | -0.019 | -0.028 | 0.28 | 0.018 |
| y_V | -0.12 | 0.019 | -0.0011 | 0.036 | -0.1 | 0.57 | 0.38 |
| α_{fan} | 16 | 24 | 51 | -16 | 19 | 51 | 12 |
| h_{min} | 4.8 | 10 | 14 | 2 | 15 | 24 | 27 |
| h_{max} | 3.2 | 4.1 | 5 | 1.8 | 5.1 | 7.3 | 11 |
| w | 1.8 | 3.5 | 5.9 | 1.1 | 3.5 | 8.1 | 7.6 |
| s | 1.6 | -1.2 | -3.5 | -6.5 | -23 | 13 | 8.5 |

Table 3: Linear terms \mathcal{B}_1 of regression coefficients, dataset of 8 varying parameters of the bracing ($\sigma = 0.2$)

| | f_1 | f_2 | f_3 | f_4 | f_5 | f_6 | f_7 |
|-----------------------|----------|----------|----------|---------|---------|----------|---------|
| α_V | 2.6 | 7.5 | -8.2 | 5.1 | 13 | 29 | 63 |
| l_V | 2.2e-05 | -0.00011 | -0.00025 | 0.00027 | 0.00016 | -0.00025 | 7.5e-05 |
| y_V | -0.00096 | 0.00094 | 0.00098 | 0.00079 | 0.001 | 0.0049 | 0.0084 |
| α_{fan} | -7.9 | -4.7 | -3.8 | 15 | -16 | 19 | -12 |
| h_{min} | -0.49 | -1.3 | -2 | 0.42 | -2 | -4.1 | -4.7 |
| h_{max} | 0.11 | 0.061 | -0.085 | 0.14 | -0.26 | -0.079 | 0.19 |
| w | -0.074 | -0.11 | -0.2 | 0.029 | -0.13 | -0.16 | -0.23 |
| s | -19 | -20 | -23 | -3.6 | 13 | -63 | -63 |

Table 4: Quadratic terms \mathcal{B}_2 of regression coefficients, dataset of 8 varying parameters of the bracing ($\sigma = 0.2$)

Bibliography

- [1] “Acoustic guitar anatomy.” <http://www.its-all-about-guitar.com/acoustic-guitar-anatomy.html>.
- [2] I. Curtu, M. D. Stanciu, N. Cretu, and I. Rosca, “Modal analysis of different types of classical guitar bodies,” in *Proceedings of the 10th WSEAS International Conference on Acoustics & Music: Theory & Applications–AMTA09 (ISTP/ISI Proceeding of Thomson Scientific-Institute for Scientific Information)*, pp. 23–25, 2009.
- [3] “Detailed explanation of the finite element method.” <https://www.comsol.com/multiphysics/finite-element-method>, 2017. COMSOL AB, Stockholm, Sweden.
- [4] T. Ono, S. Miyakoshi, and U. Watanabe, “Acoustic characteristics of unidirectionally fiber-reinforced polyurethane foam composites for musical instrument soundboards,” *Acoustical science and technology*, vol. 23, no. 3, pp. 135–142, 2002.
- [5] T. Ono and D. Isomura, “Acoustic characteristics of carbon fiber-reinforced synthetic wood for musical instrument soundboards,” *Acoustical science and technology*, vol. 25, no. 6, pp. 475–477, 2004.
- [6] N. H. Fletcher and T. D. Rossing, *The Physics of Musical Instruments*. Springer, 1998.
- [7] G. Cucuzzoli and M. Garrone, *Classical Guitar Design*. Springer, 2020.
- [8] J. A. Torres and R. R. Boullosa, “Influence of the bridge on the vibrations of the top plate of a classical guitar,” *Applied Acoustics*, vol. 70, no. 11, pp. 1371–1377, 2009.
- [9] M. Mihălcică, M. D. Stanciu, and S. Vlase, “Frequency response evaluation of guitar bodies with different bracing systems,” *Symmetry*, vol. 12, no. 5, 2020.
- [10] T. Sumi and T. Ono, “Classical guitar top board design by finite element method modal analysis based on acoustic measurements of guitars of different quality,” *Acoustical Science and Technology*, vol. 29, no. 6, pp. 381–383, 2008.

- [11] S. Šali and J. Kopač, “Positioning of braces on a guitar soundboard,” in *Proceedings of SEM, IMAC-XX: A Conference on Structural Dynamics, Los Angeles, California*, vol. 1, pp. 709–715, 2002.
- [12] P. Dumond and N. Baddour, “Effects of using scalloped shape braces on the natural frequencies of a brace-soundboard system,” *Applied Acoustics*, vol. 73, no. 11, pp. 1168–1173, 2012.
- [13] I. Curtu, M. D. Stanciu, R. Grimberg, and A. Savin, “Experimental research regarding the dynamic behaviour of the classical guitar,” in *Proceedings of the 10th WSEAS international conference on Acoustics & music: theory & applications*, pp. 53–58, 2009.
- [14] G. Paiva and J. Dos Santos, “Modal analysis of a brazilian guitar body,” in *Proceedings of the ISMA International Symposium on Music Acoustics*, pp. 233–239, 2014.
- [15] R. Corradi, P. Fazioli, S. Marforio, A. Paluella, F. Ripamonti, and G. Squicciarini, “Modal analysis of a grand piano soundboard,” in *International conference on noise and vibration engineering (ISMA 2010)*, 2010.
- [16] G. Caldersmith, “Designing a guitar family,” *Applied Acoustics*, vol. 46, no. 1, pp. 3–17, 1995. Musical Instrument Acoustics.
- [17] M. Pavlidou, *A physical model of the string-finger interaction on the classical guitar*. PhD thesis, University of Wales, Cardiff, 1997.
- [18] P. Roch, *A Modern Method for the Guitar (School of Tarrega)*. G. Schirmer, 1921.
- [19] R. M. French, *Engineering the Guitar: Theory and Practice*. Springer, 2010.
- [20] E. Skrodzka, A. Łapa, B. B. J. Linde, and E. Rosenfeld, “Modal parameters of two incomplete and complete guitars differing in the bracing pattern of the soundboard,” *The Journal of the Acoustical Society of America*, vol. 130, no. 4, pp. 2186–2194, 2011.
- [21] E. Jansson, *Acoustics for violin and guitar makers*. Kungl. Tekniska högskolan, Department of Speech. Music and Hearing, 2002.
- [22] T. R. Moore and S. A. Zietlow, “Interferometric studies of a piano soundboard,” *The Journal of the Acoustical Society of America*, vol. 119, no. 3, pp. 1783–1793, 2006.
- [23] E. Jansson, N.-E. Molin, and H. Sundin, “Resonances of a violin body studied by hologram interferometry and acoustical methods,” *Physica Scripta*, vol. 2, pp. 243–256, dec 1970.

- [24] R. Viala, M. A. Pérez, V. Placet, A. Manjón, E. Foltête, and S. Cogan, “Towards model-based approaches for musical instruments making: validation of the model of a spanish guitar soundboard and characterization features proposal,” *Applied Acoustics*, vol. 172, p. 107591, 2021.
- [25] E. Jansson, I. Bork, and J. Meyer, “Investigations into the acoustical properties of the violin,” *Acta Acustica united with Acustica*, vol. 62, no. 1, pp. 1–15, 1986.
- [26] T. J. Hughes, *The finite element method: linear static and dynamic finite element analysis*. Courier Corporation, 2012.
- [27] “Structural mechanics module v. 5.6.” <https://doc.comsol.com/5.6/doc/com.comsol.help.sme/StructuralMechanicsModuleUsersGuide.pdf>. COMSOL AB, Stockholm, Sweden.
- [28] “What is structural mechanics? - an introductory guide.” <https://www.comsol.com/multiphysics/introduction-to-structural-mechanics>. COMSOL AB, Stockholm, Sweden.
- [29] L. Frignani, A. Radice, and T. Rizzi, *The guitar in Italy*. LF Edizioni, 2015.
- [30] K. Coates, *Geometry and proportion and the art of lutherie: a study of the use and aesthetic significance of geometry and numerical proportion in the design of European bowed-and plucked-string instruments in the sixteenth, seventeenth...* PhD thesis, Royal College of Art, 1979.
- [31] J. D’Errico, “interparc.” <https://www.mathworks.com/matlabcentral/fileexchange/34874-interparc>, 2020. MATLAB Central File Exchange.
- [32] S. McKinley and M. Levine, “Cubic spline interpolation,” *College of the Redwoods*, 1998.
- [33] R. J. Ross, *Wood Handbook*. USDA, FPL-GTR-190, 2010.
- [34] D. Salvi, “Modal analysis and optimization of the top plate of string instruments through a parametric control of their shape,” Master’s thesis, Politecnico di Milano, Milano, I, october 2020.
- [35] “How to use coordinate-based selections.” <https://www.comsol.com/learning-center/coordinate-based-selections-model-setup>. COMSOL AB, Stockholm, Sweden.

- [36] H. Wright, *The acoustics and psychoacoustics of the guitar*. PhD thesis, Cardiff, 1998.
- [37] “Matlab mathematics.” https://www.mathworks.com/help/pdf_doc/matlab/matlab_math.pdf, 2020. The MathWorks, Natick, MA, USA.
- [38] J. D’Errico, “polyfitn.” <https://it.mathworks.com/matlabcentral/fileexchange/34765-polyfitn>, 2021. MATLAB Central File Exchange.
- [39] X. Zhou, X. Liu, and G. Hu, “Elastic metamaterials with local resonances: an overview,” *Theoretical and Applied Mechanics Letters*, vol. 2, no. 4, p. 041001, 2012.
- [40] A. Nateghi, L. Sangiuliano, C. Claeys, E. Deckers, B. Pluymers, and W. Desmet, “Design and experimental validation of a metamaterial solution for improved noise and vibration behavior of pipes,” *Journal of Sound and Vibration*, vol. 455, pp. 96–117, 2019.
- [41] “Comsol multiphysics $\text{\textcircled{R}}$ v. 5.6.” www.comsol.com. COMSOL, Inc.
- [42] K. Patil, J. Baqersad, D. Ludwigsen, and Y. Dong, “Extracting vibration characteristics of a guitar using finite element, modal analysis, and digital image correlation techniques,” in *Proceedings of Meetings on Acoustics 172ASA*, vol. 29, p. 065003, Acoustical Society of America, 2016.